



Universiteit  
Leiden  
The Netherlands

## **The immune compartment at the maternal-fetal interface throughout human pregnancy**

Zwan, A. van der

### **Citation**

Zwan, A. van der. (2020, February 6). *The immune compartment at the maternal-fetal interface throughout human pregnancy*. Retrieved from <https://hdl.handle.net/1887/84689>

Version: Publisher's Version

License: [Licence agreement concerning inclusion of doctoral thesis in the Institutional Repository of the University of Leiden](#)

Downloaded from: <https://hdl.handle.net/1887/84689>

**Note:** To cite this publication please use the final published version (if applicable).

Cover Page



Universiteit Leiden



The handle <http://hdl.handle.net/1887/84689> holds various files of this Leiden University dissertation.

**Author:** Zwan, A. van der

**Title:** The immune compartment at the maternal-fetal interface throughout human pregnancy

**Issue Date:** 2020-02-06

# Chapter 07

Visualizing dynamic changes at the  
maternal-fetal interface throughout human  
pregnancy by mass cytometry

Anita van der Zwan, Vincent van Unen, Guillaume Beyrend,  
Sandra Laban, Carin van der Keur, Hanneke J.M. Kapsenberg,  
Thomas Höllt, Michael Eikmans, Susana M. Chuva de Sousa Lopes,  
Marie-Louise P. van der Hoorn, Frits Koning,  
Frans H.J. Claas, Sebastiaan Heidt

Submitted

## **Abstract**

During healthy pregnancy, a balanced microenvironment at the maternal-fetal interface with coordinated interaction between various immune cells is necessary to maintain immunological tolerance. While specific decidual immune cell subsets have been investigated, a system-wide unbiased approach is lacking. Here, mass cytometry was applied for data-driven, in-depth immune profiling of the total leukocyte population isolated from 1st, 2nd and 3rd trimester decidua, as well as maternal peripheral blood at time of delivery. The maternal-fetal interface showed a unique composition of immune cells, different from peripheral blood, with significant differences between early and term pregnancy samples. It revealed substantial heterogeneity in the decidual lymphoid and myeloid cell lineages that shape gestational-specific immune networks and putative differentiation trajectories over time during gestation. Uncovering the overall complexity at the maternal-fetal interface throughout pregnancy resulted in a human atlas that may serve as a foundation upon which comprehension of the immune microenvironment and alterations thereof in pregnancy complications can be built.

## Introduction

Preserving immunological tolerance towards the semi-allogeneic fetus during pregnancy while providing protection against environmental pathogens relies on intricately regulated local and systemic immune adaptations. Direct contact between the mother and the fetus exists at the decidua basalis, located at the implantation site, and at the decidua parietalis that is part of the membranes which line the uterine cavity and surround the fetus. Fetal extravillous trophoblasts (EVT) migrate into the maternal decidua early during pregnancy (1), and express HLA-C, -G, -E and -F but lack expression of the classical HLA-A and -B antigens, rendering them in part invisible to natural killer (NK) cells and the large majority of maternal allogeneic CD8<sup>+</sup> T cells (2, 3, 4). In concert, alterations in both the maternal innate and adaptive immune compartment occur, where NK and innate lymphoid cells (ILC) prevail in early pregnancy, while T cell proportions increase over the course of gestation. Antigen-presenting cell (APC) numbers remain relatively constant throughout pregnancy while B cells have been described as a sparse population (5, 6, 7, 8).

Yet, the fetus is not completely protected as maternal NK cells can recognize fetal HLA-C and HLA-G and fetal-specific CD8<sup>+</sup> and CD4<sup>+</sup> T cells have been observed in maternal peripheral blood and decidua (9, 10, 11, 12). As such, aberrant regulation of the maternal immune system has been suggested to play a role in pregnancy complications, such as pre-eclampsia (13, 14), recurrent miscarriages (15, 16), preterm birth (17, 18, 19), and fetal growth restrictions (20). Incomplete understanding of the maternal-fetal interface during a healthy pregnancy has hampered the systematic investigation of major pregnancy complications. Most work in the field of reproductive immunology has focused on individual subsets of decidual immune cells while a comprehensive, system-wide approach that visualizes all decidual immune cell lineages at different time points during pregnancy is lacking. High-dimensional single-cell technologies such as mass cytometry (21) now allow an in-depth and unbiased data-driven analysis of the composition of the immune system at the maternal-fetal interface.

In the current study, we applied two mass cytometry antibody panels, one to detect heterogeneity within all major immune cell lineages while the other with a focus on T cell-specific markers, to determine the composition of the maternal immune compartment in first, second and third (term) trimester decidual samples as well as maternal PBMC (mPBMC) at the time of delivery. Our results provide an immune atlas of the maternal-fetal interface in healthy pregnancy that may serve as a foundation for improved understanding of pregnancy complications.

## Results

### **The maternal-fetal interface harbors a unique immune cell composition**

We analyzed first, second and third trimester decidual samples along with mPBMC taken at the time of delivery and PBMC of non-pregnant age-matched women (NP PBMC) as a control (Table 1). A general mass cytometry panel comprising 39 antibodies (Table 2) was used to provide a broad coverage of the myeloid and lymphoid immune compartments. For in-depth profiling of the T cell compartment, a second panel comprising 37 antibodies (Table 3) was applied. After data acquisition (Table 4), live, single CD45+ cells were selected for downstream analysis (Fig. S1A, Fig. 1A). Conventional cell populations were verified by manual gating and have previously been validated (22). At several timepoints during the acquisition timeline, a PBMC reference sample was included and corroborated reproducible staining and acquisition among different sets of experiments (Fig. S2A, B). To allow systematic comparison of samples, the data obtained with the general panel (49 samples;  $19 \times 10^6$  CD45+ cells) and the data obtained with the T cell panel (44 samples;  $17 \times 10^6$  CD45+ cells) were pooled separately and analyzed with HSNE and t-SNE in Cytosplore (23, 24). Comparison of the absolute numbers and percentages of CD45+ cells and correlations thereof showed a similar pattern in the general and T cell panel (Fig. S1B, C).

At the overview level, the HSNE landmarks depicted the global data heterogeneity and marker expression profiles in both panels and identified the major immune cell subsets of myeloid cells, ILC, CD4+ T cells, CD8+ T cells (including the TCR $\gamma\delta$  lineage), and B cells (Fig. 1B, Fig. S1D). Subsequently, t-SNE analysis based on cell frequencies separated the samples of 1st and 2nd trimester from samples of term basalis and parietalis, and peripheral blood, indicative of distinct immune profiles (Fig. 1C, Fig. S1E). Cell frequencies of the major immune cell lineages confirmed ILC, primarily NK cells, as being the predominant cell type in 1st trimester, decreasing towards the end of pregnancy, and contrasting the dynamics of T cells. This analysis also validated that the number of myeloid cells remains relatively constant throughout gestation, while B cells are hardly present (Fig. 1D, Fig. S1F) (5).

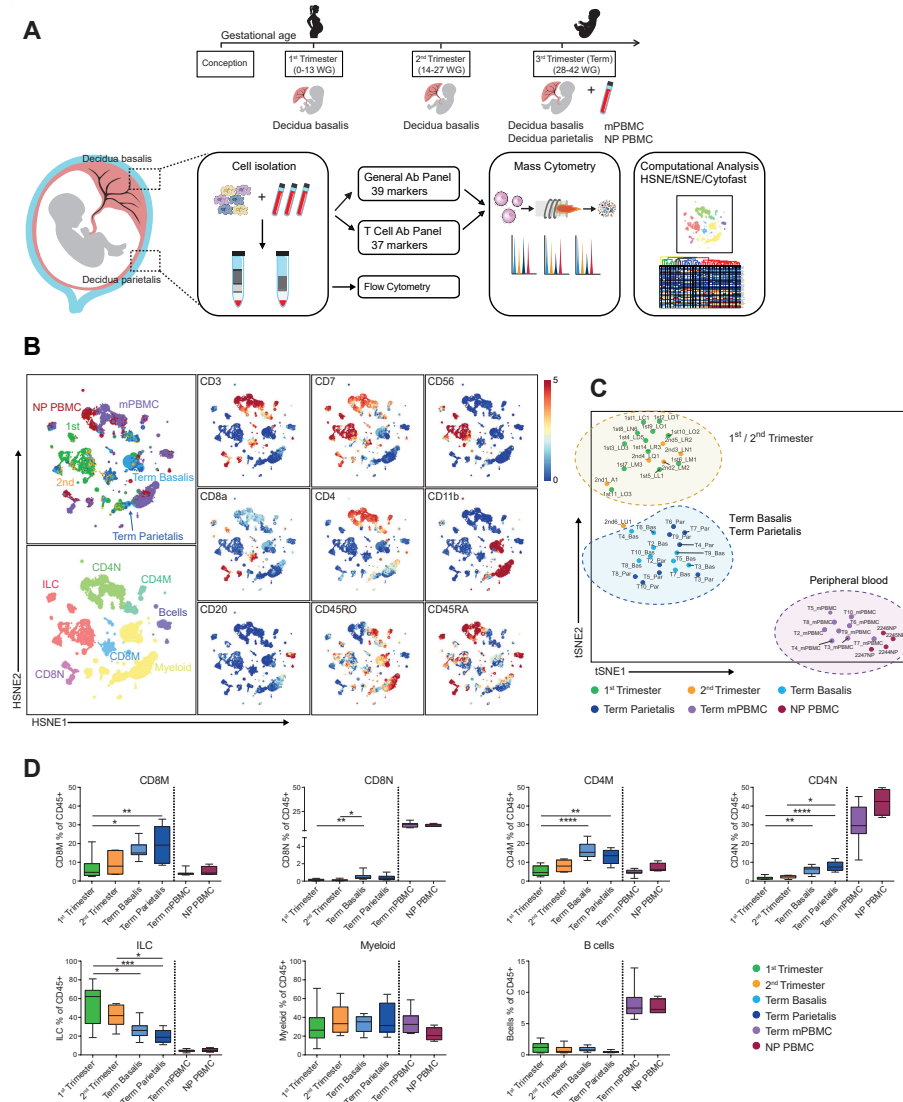


**Figure 1. Identification of major immune cell lineages at the maternal-fetal interface.** (A) Experimental setup. First (6-13 weeks of gestation, WG), second (14-18WG) and third trimester (term; > 38WG; basalis and parietalis) decidual samples along with maternal peripheral blood mononuclear cells (mPBMC) and non-pregnant PBMC (NP PBMC) were analyzed. (B) First-level HSNE visualization of the major immune cell lineages derived from decidua and peripheral blood. Colors top left indicate tissue type (1st trimester n = 12; 2nd trimester n = 6; term basalis and parietalis n = 9; mPBMC n = 9; NP PBMC n = 4); colors bottom left indicate major immune cell types (CD8M, CD8 memory T cells; CD8N, CD8 naïve T cells; CD4M, CD4 memory T cells; CD4N, CD4 naïve T cells; ILC, innate lymphoid cells); colors for plots on the right indicate the arcSinh5-transformed expression values of the specified markers where every dot represents a landmark. Memory and naïve clusters were distinguished based on CD45RO and CD45RA expression. (C) t-SNE visualization of the separation between decidual and peripheral blood samples (as percentage of CD45+ cells). Every dot represents a single sample. (D) Major immune cell lineages (as percentage of CD45+ cells) throughout gestation and within mPBMC and NP PBMC. Boxplots depict the 10-90 percentile and the Kruskal-Wallis with Dunn's test for multiple comparisons was applied. \*P < 0.05; \*\*P < 0.01; \*\*\*P < 0.001; \*\*\*\*P < 0.0001.

### **Early pregnancy reveals a heterogeneous group of myeloid cells with high HLA-DR expression**

Next, for each antibody panel, the data from all decidual samples were pooled and HSNE analysis was performed on every lineage individually. Within the myeloid cell lineage (Fig. S2C), the second hierarchical level revealed six large subpopulations that could be discriminated based on differential expression of CD14, CD11c, CD11b, HLA-DR, CD16, and CD15 (Fig. S2D, E). Subsequently, Gaussian mean-shift clustering was applied and quantified with Cytofast (25), revealing 16 phenotypically distinct myeloid cell clusters (Fig. 2A). Here, HSNE overview plots showed the individual markers that contributed to the separation into distinct clusters (Fig. 2B). Next, we determined which myeloid cell clusters were differentially present in 1st and 2nd trimester, term basalis, and term parietalis samples to uncover dynamics throughout pregnancy (Fig. 2C). Only cell clusters with significant differences (false discovery rate (FDR) < 5%) between the groups are shown.

Notably, early pregnancy was characterized by the presence of a heterogeneous group of myeloid cells with high HLA-DR expression. CD163+HLA-DR+ cells, also expressing intermediate levels of CD56 and CD7 (cluster 'Other CD56+CD163+'), were observed in the 1st and 2nd trimester (Fig. 2C), and may represent myeloid-like NK cell progenitors. Furthermore, cell clusters of decidual mononuclear phagocytes (dMP), namely dMP1, dMP2, dMP5, and dMP6, expressing various combinations of CD14, CD11b, CD11c, CCR6, CD38, and CD69 were more prominent in 1st and 2nd trimester decidua compared to term decidua. The immune-regulatory CD163+ M2 macrophage (M $\phi$ ) subtype, was present in early pregnancy and term decidua parietalis, but hardly in term decidua basalis. In addition, CD11c<sup>high</sup>CD14-CD16- Mo-DC were predominantly abundant in 1st trimester. Moreover, CCR6+CD45RA+CD38- dMP cell clusters with low HLA-DR expression (dMP3 and dMP4) were dominantly present in term decidua basalis while the largest population of CD15+CD16+ granulocytes was found in both term decidua basalis and parietalis (Fig. 2C). Finally, a clear separation between early and late pregnancy samples in unsupervised principal component analysis (PCA; Fig. 2D) was driven by an abundance of granulocytes in late pregnancy and supported by a previously unrecognized diverse composition of myeloid cells in early pregnancy.

Together, these results reveal substantial changes in the composition of the myeloid compartment during gestation.

### **Dynamic changes in the composition of the ILC compartment during pregnancy**

A similar analysis of the ILC compartment (CD3-CD7+) confirmed its well-described cellular composition in decidua (26). The general panel classified 14 clusters with high expression of CD56 and lack of CD16 (Fig. S3A). Early pregnancy was characterized by activated CD161+CD122+NKp46+CD107+CD69+ NK cells, tissue-resident CD69+CD103+ cell clusters and ILC-3 (Fig. S3A, B), coupled to the expression of CD39 and TIM-3 (Fig. S3C,

D, E) (27). Towards the end of pregnancy, NK cells displayed a less activated phenotype with lower expression of CD161, CD122, NKp46 and CD103, and higher expression of CD45RA and CD16 (mostly in term basalis; Fig. S3B). Tissue-resident-like ILC were not only observed in 1st trimester (dIC6; decidual ILC Cluster), but also in small numbers in term samples (dIC1) along with the expression of TIGIT (Fig. S3C, D). In addition, expression of the co-inhibitory receptors TIM-3 and CD39 was observed in both early and term parietalis samples. NK2, NK3, and NK5 clusters resembled a phenotype similar to the intermediate innate subset described in fetal intestine that can differentiate into ILC3 and NK cells (28).

High proportions of activated ILC are present early in pregnancy alternated by dissimilar, smaller proportions of ILC cell clusters in term pregnancy, where the largest separation was observed between 1st trimester and term basalis (Fig. S3F).

### **The decidua harbors NKT-like TCR $\gamma\delta$ cells**

Substantial phenotypic diversity was observed within decidual TCR $\gamma\delta$  cells where seven cell clusters were identified within the general panel (Fig. S4A, B). The most prominent cell clusters were CD161+KLRG1+ TCR $\gamma\delta$ EM, present throughout gestation, and CD69+TCR $\gamma\delta$ EMRA that were dominant in term basalis. Remarkably, NKT-like populations of TCR $\gamma\delta$  cells expressing CD56 and CD11c were also observed. TEMRA, with high expression of CD45RA, and TEM cell clusters persisted in early pregnancy while cells co-expressing CD45RA and CD45RO and positive for CD27, CD5 and CD69 increased in term parietalis (Fig. S4A, C). Even though differences throughout gestation were existent, close clustering between the three different trimesters was observed in a PCA (Fig. S4D).

### **CD4+ T cell characterization reveals unexplored diversity within memory and regulatory phenotypes**

In the CD4+ T cell lineage 17 cell clusters were identified: one naïve (N; CD45RA+CCR7+), two terminally differentiated (TEMRA; CD45RA+CCR7-), one central-memory (CM; CD45RO+CCR7+), seven effector-memory (EM; CD45RO+CCR7-), one CD45RA+RO+ and five memory regulatory-like T cell (Treg-like; CD25+CD127-) clusters (Fig. 3A, B). Early in pregnancy, natural-killer-like CD4+ T cells (NKT-like) exist that express CD56, CD11c, CD161, CD122, NKp46, and CD38 (Fig. S5A, Fig. 3C). Expression of CD127 and CCR6 occurred towards the end of pregnancy (T2EM), consistent with the early pregnancy-associated T4EM cluster that lacked expression of these markers. At term, CD4+CD7-CD161+ TEM cells expressing CD27 and CCR6 (T2EM) were observed in term basalis, whereas CD4+CD7+CD161- TEM cells expressing CD38 and ICOS, and lacking CCR6 (T7EM) were predominantly present in term parietalis (Fig. 3C). Furthermore, CD4+ TEM cells showed co-expression of PD-1 and ICOS, at lower levels than the Treg-like population, and lack of TIGIT and CD39.

Considerable heterogeneity within the Treg-like compartment was uncovered, where

CD25+CD127- cell clusters expressed high levels of co-inhibitory (PD-1, CD39, TIGIT) and stimulatory (ICOS, CD38, CD28, CD27) receptors, including co-expression thereof (Fig. 3A, B). When investigating the Treg-like compartment in more detail, previously unrecognized heterogeneity was observed with respect to the expression of the Treg-associated markers TIM-3, CCR8, and CCR4 (Fig. S5B) (29, 30, 31). Tr1 cells, identified by co-expression of LAG-3 and CD49b (32), were observed in mPBMC but absent in decidual CD4+ T cells. Quantification of the presence of these CD25+ cell clusters in the gestational age groups revealed that T4REG (HLA-DR-CD69-PD-1-) and T3REG (CCR4+CD38+) were more frequent in early pregnancy and lower in term basalis, whereas the largest Treg-like population, T2REG (ICOS+PD-1+TIGIT+CD39+), was significantly increased in term parietalis (Fig. 3C). Furthermore, T5REG (CCR6+ICOS+TIGIT+PD-1-CD39-) was significantly increased in term decidua basalis and parietalis, while virtually absent in early pregnancy. By aligning cells from these five Treg-like clusters along a two-dimensional diffusion map (33), putative differentiation and/or plasticity trajectories were observed between cell clusters T2REG, T3REG, T4REG, and T5REG. T1REG, the smallest Treg-like cluster, was distinct owing to the lack of CD7 and CD27 expression (Fig. S5C).

To evaluate the Treg-like phenotypes further, intracellular expression of FOXP3, HELIOS, and CTLA-4 in CD4+CD25+CD127- and CD127+ T cells was assessed by flow cytometry in decidual samples (Table 5). Co-expression of FOXP3, HELIOS, CTLA-4, CD39, ICOS, and TIGIT was observed in HSNE analysis of flow cytometry data, confirming a valid regulatory T cell phenotype (Fig. 3D). In addition, differential co-expression of these markers was observed in several cell clusters, where not all CD4+CD25+CD39+ICOS+ cells expressed FOXP3 and/or HELIOS. This indicates that the Treg-like CD25+CD127- populations detected by mass cytometry represent a heterogeneous group of Treg and Treg-like cells at the maternal-fetal interface (Fig. 3D). Flow cytometry data revealed an increase in CD4+CD25+CD127+ T cells, known to be activated effector CD4+ T cells (34), and regulatory-like CD4+CD25+CD127- T cells towards the end of pregnancy, with this increase being most apparent in term parietalis (Fig. 3E, Fig. S5D). These data uncovered distinct CD4+ T cell populations, where clear separation is not only portrayed between early versus term pregnancy, but also between term basalis versus parietalis (Fig. 3F).

Next, diffusion mapping was used to distinguish prospective relationships among the different types of memory CD4+ T cell clusters. Two-dimensional diffusion plots revealed a split into two branches with T4EM, lacking CD127 expression, at the center of the split (Fig. 4A). Gradients of protein expression between cells were observed rather than discrete cell clusters (Fig. 4B). The branch that expanded along diffusion component 2 (DC2) consisted of CD7+CD161+ and CD161- TEM cells that were CD127+ and CD27+. TCM was projected at the end of this trajectory branch. The second branch along DC1 consisted of the CD7-CD161+ clusters that showed CD127 expression, including one

cluster (T3EM) that lacked CD27 expression. The two EMRA clusters separated out from the EM clusters based on their expression of CD45RA and lack of CD27 expression. These results suggest putative differentiation states between the identified EM CD4+ T cell clusters throughout pregnancy.

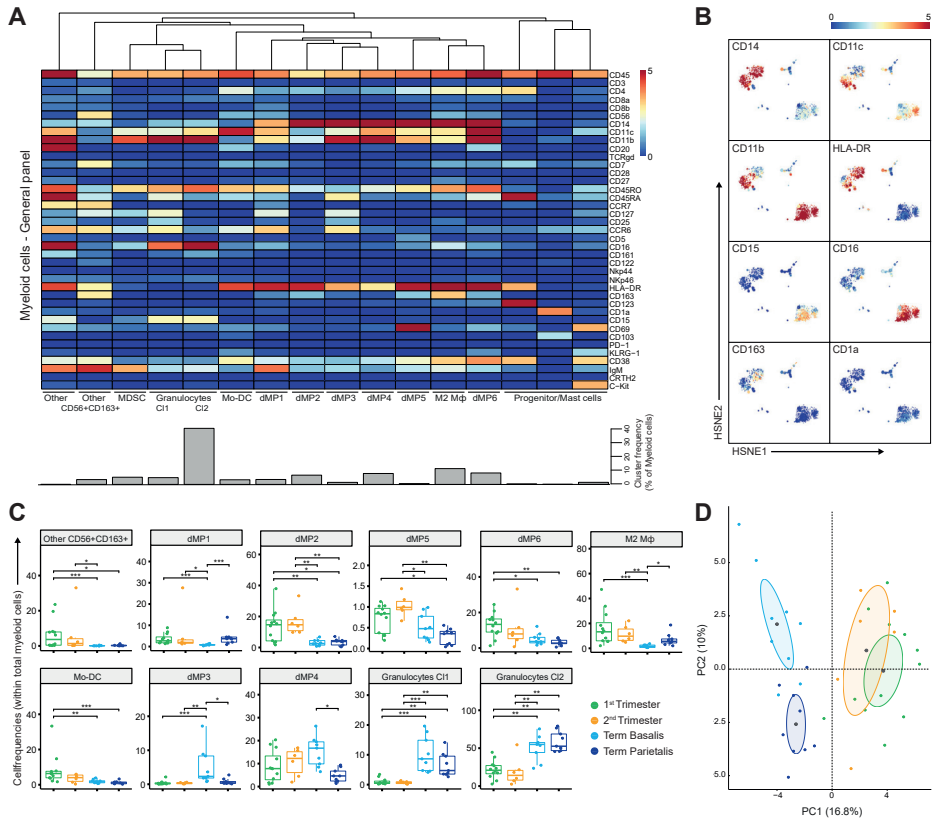


**Figure 2. The myeloid compartment is highly diverse in early pregnancy.**

(A) Heatmap showing the median arcSinh-transformed marker expression values for the 16 identified myeloid clusters within the general panel (36 samples; 2,390,451 cells). Cluster IDs and cluster frequencies are displayed at the bottom of the heatmap. (B) First-level HSNE embedding of the arcSinh5-transformed expression values of the indicated markers (note these are the same plots as in Fig. S2E). (C) Boxplots of sample frequencies, divided per trimester, of the cell clusters plotted as a fraction of total myeloid cells. The Kruskal-Wallis with Dunn's test for multiple comparisons was performed and only clusters with significant differences (false discovery rate (FDR) < 5%) between the groups are shown. (D) Unsupervised principal component analysis (PCA) of the sample frequencies (as percentage of total myeloid cells), where the gestational age groups are depicted along the first two components. The centroid of each group is indicated in grey. MDSC, myeloid-derived suppressor cells; dMP, decidual mononuclear phagocytes; M, macrophage. \*P < 0.05; \*\*P < 0.01; \*\*\*P < 0.001.



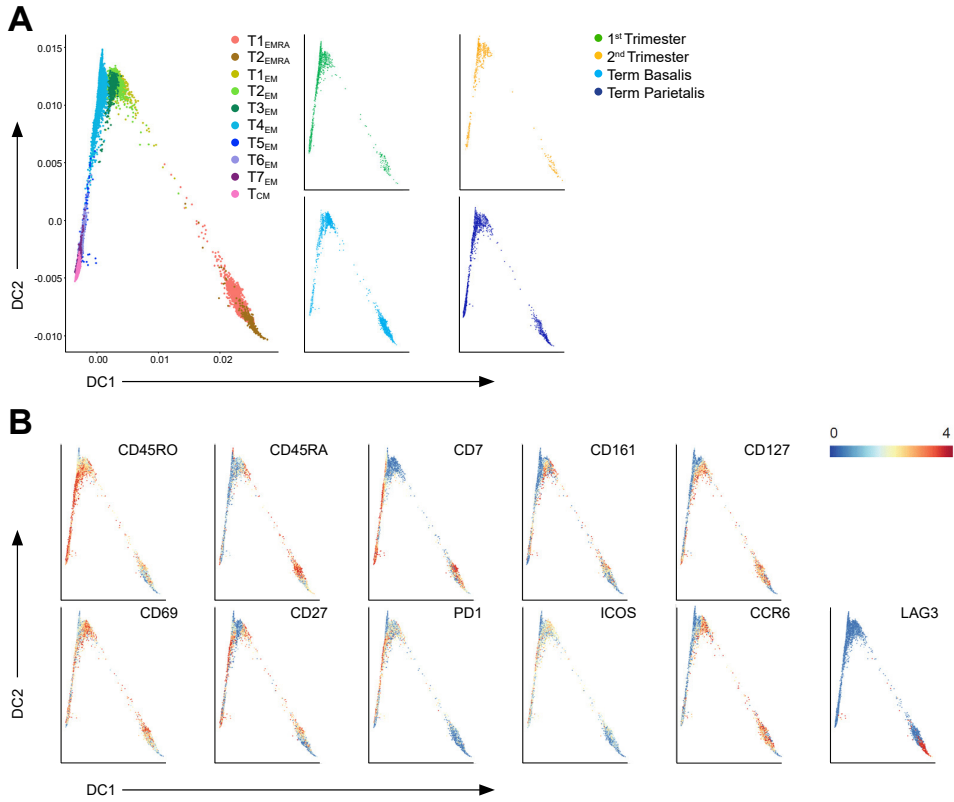


**Figure 4. Trajectory analysis of effector and memory decidual CD4+ T cells.**

(A) Visualization of terminally differentiated (EMRA) and effector-memory (EM) CD4+ T cell clusters in a diffusion map along two components. Each color in the left panel represents a cluster of cells. In the right panel, cells within the 1st trimester, 2nd trimester and term decidua basalis and parietalis are portrayed. (B) ArcSinh5-transformed expression values of the specified markers in the diffusion map.

**Decidual CD8+ T cells co-express inhibitory and stimulatory receptors**

We next investigated the heterogeneity within the CD8+ T cell compartment where 20 CD8+ T cell clusters were characterized, namely one naïve, seven TEMRA, five EM, and seven clusters co-expressing CD45RA and CD45RO, a phenotype that is associated with proliferation (Fig. 5A, B). Four of these clusters revealed significant differences between the decidual samples (Fig 5C). The tissue-resident memory (TRM) CD8+ T cell cluster T4RORA (CD69+CD103+CD38+CD161+PD-1+CD39+) was more frequent in early pregnancy, while T5EMRA (CD69<sup>high</sup>) and T6RORA (CD127+CCR6+CD38+CD69+) were more abundant in term samples. Also, T4EMRA (CD127+CCR6+) was increased in term basalis. In addition, a trend for a higher presence of NKT1-like cells in the 1st trimester, a gradual increase in NKT3-like and T5RORA cells from 1st trimester to term, and higher numbers of T2RORA in 1st trimester and term basalis were observed (Fig 5C, Fig. S6A). High levels of CD27 were observed in several effector and effector-memory cell clusters (e.g. T5EMRA, T5RORA, T6RORA).

Where our recent work demonstrated a mixed gene expression signature of activation and dysfunction in bulk memory decidual CD8+ T cells (35), mass cytometry at the single-cell level revealed the expression of inhibitory and stimulatory receptors to be intertwined (Fig. 5A). This co-expression of inhibitory (CD39, PD-1, TIGIT) and stimulatory (ICOS, CD69, CD27) receptors was verified by flow cytometry and mainly observed in term basalis and parietalis (Fig. S6B). Interestingly, the TEMRA and TCM clusters within the CD8+ T cell compartment contrasted the frequencies of these populations within the CD4+ T cell compartment with a higher percentage of TEMRA and lower percentage of TCM within the CD8+ T cells (Fig. S6C). In general, the differences in marker expression in the CD8+ T cell compartment were more subtle when compared to the CD4+ T cells. Consequently, the PCA showed a less clear separation between early and late pregnancy with term parietalis being more similar to 1st and 2nd trimester samples than term basalis (Fig. 5D).

In a two-dimensional diffusion plot analysis two branches were observed with the CD38-clusters (T5EMRA, T5RORA) at the center of the split. Here, the CD38+CD69+ TEMRA and TEM clusters expanded along DC1, while the TRM cells and CD127+CCR6+ TEM cells expanded along DC2 (Fig. 5E, F). Furthermore, along DC2 cell clusters T5EMRA, T5RORA, and T6RORA with lower expression of CD45RO and PD-1 and high expression of CD69, were absent in early pregnancy and appeared in term pregnancy, as observed in Fig. 5C (Fig. 5E; dashed circle). These potential differentiation trajectories suggest a phenotypic continuum and thereby possible plasticity between specific CD8+ T cell clusters.

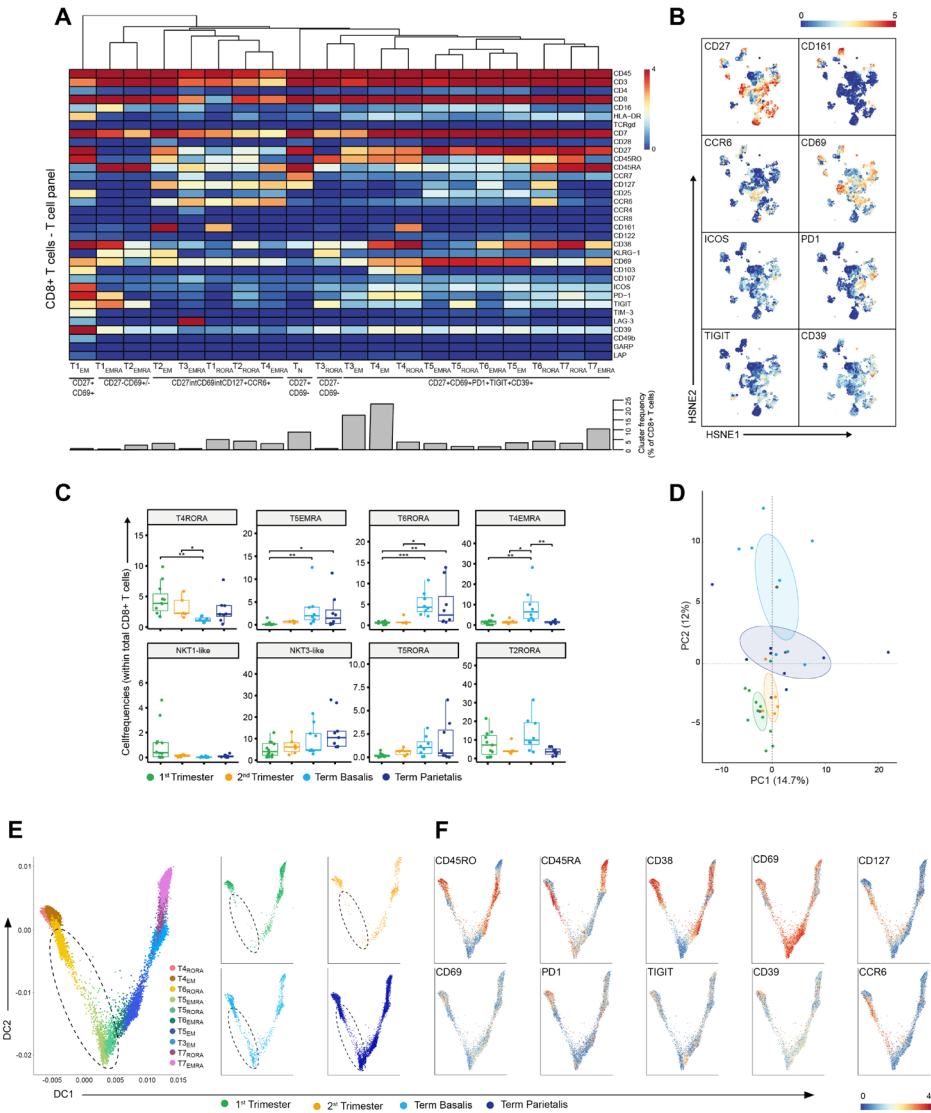


**Figure 5. In-depth characterization of the heterogeneity within the CD8+ T cell compartment.**

(A) Heatmap showing the marker expression values for the 20 identified CD8+ T cell clusters within the T cell panel (32 samples; 707,147 cells). Cluster IDs and cluster frequencies are displayed at the bottom of the heat map. (B) First-level HSNE embedding of the expression values of the indicated markers. (C) Boxplots of sample frequencies, divided per trimester, of the clusters plotted as a fraction of total CD8+ T cells. The Kruskal-Wallis with Dunn's test for multiple comparisons was performed. (D) PCA of the sample frequencies (as percentage of total CD8+ T cells) where the gestational age groups are depicted along the first two components. The centroid of each group is indicated in grey. (E) Visualization of TEMRA, TRORA and TEM CD8+ T cell clusters in a diffusion map along two components. Each color in the left panel represents a cluster of cells. In the right panel, cells within the 1st trimester, 2nd trimester and term decidua basalis and parietalis are portrayed. (F) ArcSinh5-transformed expression values of the specified markers in the diffusion map. \*  $P \leq 0.05$ ; \*\*  $P \leq 0.01$ ; \*\*\*  $P \leq 0.001$ .

**B cells are mainly present early in pregnancy**

Although the number of B cells was low, nine CD20+ B cell clusters with variable expression of CD38, CD27 and IgM were identified within the general panel (Fig. S7A). Interestingly, most B cells were detected in the 1st trimester (Fig. S7B). CD20 was also included in the T cell panel (as exclusion marker) and showed to be useful in detecting CD39 expression on several B cell clusters (Fig. S7C).

**Correlation analysis reveals gestational-specific immune networks**

To conflate the 77 identified immune cell clusters within the general panel and visualize relationships between them, a correlation network analysis was performed using the sample frequencies. This analysis demonstrated that 73% of clusters were strongly correlated with each other (Spearman rank > 0.7; Fig. 6A). Subsequently, multivariate associations between individual and groups of clusters were detected by applying a multinomial logistic regression model with the global test (Fig. 6B) (36, 25). Four networks were revealed in which colored nodes highlight the significance of individual cell clusters in one of the four gestational age groups. Cell clusters in network 1 consisted of myeloid cells, CD4+ T cells, CD8+ T cells, and B cells, and did not reveal significant gestational specificity. Network 2 revealed a correlation between NKT-like, B cell, and NK cell clusters (including tissue-resident-like phenotypes), most of which were significantly abundant in the 1st trimester. This may reflect unappreciated interactions between NK cells and NKT-like cells early in pregnancy. Network 3 is characterized by clusters predominantly present in term basalis and included a correlation between innate immune cells such as NK cell clusters, dMP3 and granulocytes, and adaptive immune cells including TN, TEM and Treg-like CD4+ clusters, CD8+ TRORA cells, and TCR $\gamma\delta$ EMRA cells. Interestingly, a different network of clusters was observed in term parietalis (network 4), where CD4+ and CD8+ TN cells, CD4+CD127+CD161- TCM cells, CD4+ Treg-like clusters, CD8+ TEM and NKT-like cells, and TCR $\gamma\delta$  cells were correlated. These results underline that distinct immune cell interactions in basalis versus parietalis contribute to the microenvironment in term pregnancy. Thus, three of the four networks correlated with either gestational age or tissue location.



## Discussion

To better understand the maternal immune landscape throughout healthy pregnancy, we performed mass cytometry analysis of immune cells isolated from decidua throughout the three trimesters of pregnancy, and compared this to term mPBMC. This provides an unbiased, data-driven overview of all decidual immune cell populations throughout pregnancy. Next to validating previously described immune cell subsets (6, 37, 38, 39), we observed previously unrecognized immune cell heterogeneity in the decidua at different stages during pregnancy. It is plausible that the various phenotypically distinct cell clusters may be differentiation stages between cell populations, as suggested by our diffusion mapping data. Distinct clusters of dMP were detected in early pregnancy, suggestive of an essential role for antigen presentation and thereby interaction with other immune cells at the initiation of pregnancy. Furthermore, the presence of different dMP cell clusters in term basalis and parietalis may reflect distinct local antigen presentation and function. Proportions of the dMP cells decrease over gestation accompanied by an influx of granulocytes at time of parturition, in line with the observed increase in the numbers of circulating neutrophils during pregnancy (40). ILC that play an important role in early pregnancy by facilitating spiral artery remodelling and trophoblast invasion, may in small proportions preserve their function (e.g. play a role in the clearance of infections) in term pregnancy where they display a less activated phenotype with the expression of inhibitory and tissue-residency receptors.

Most studies on decidual Treg have thus far focused on CD4+FOXP3+ T cells (41, 42, 16). Our present mass and flow cytometry data confirmed the presence of other, recently described, FOXP3<sup>low/-</sup> decidual Treg subtypes (43). In addition, we observed unprecedented heterogeneity, with co-expression of inhibitory and stimulatory receptors and clusters lacking expression of FOXP3 and/or HELIOS, revealing a mixed population of Treg and Treg-like cells. It supports the hypothesis that both natural (nTreg) and induced Treg (iTreg) play a role, where bright expression of CD25 is not a prerequisite for Treg function and a decrease in FOXP3 and HELIOS expression towards term suggests a decline of nTreg and increase of iTreg throughout gestation (43). These Treg populations are induced, among others, by EVT and decidual M $\phi$  (43), and may therefore have distinct cellular targets, which likely include the formerly unexplored heterogenous group of memory CD4+ T cells. Evidence exists that 1st trimester decidual CD4+ T cells have transcriptional profiles compatible with antigen-induced activation and proliferation (44). Moreover, decidual CD4+ T cells isolated from term decidua showed fetal antigen-specific responses that were enhanced upon depletion of CD25+CD127- Treg (12). Presence of paternal antigen-specific Treg have been suggested (45), and clonal expansion of both decidual Treg (46) and memory CD4+ T cells by locally presented antigens is suggested by preliminary data from our laboratory showing a restricted CDR3

length distribution of the TCRV $\beta$  repertoire in term decidua CD4+ T cells compared to peripheral CD4+ T cells (data not shown). The observed increase in activated CD4+ T cells may be counteracted by an increase in Treg in term decidua to secure success of pregnancy. Evidently functional assays are necessary to further explore the co-existence of these memory CD4+ T cells with nTreg and iTreg, especially in the context of complicated pregnancies (47). Treg may also be essential in the regulation of distinct CD4+ and CD8+ NKT-like clusters in early pregnancy, as suggested by the increased percentages of NKT cells observed in women with unexplained recurrent spontaneous abortions (48).

Recent research on fetal-specificity (12), virus-specificity (49) and possible cross-reactivity of decidua CD8+ T cells with HLA-C (50), complemented by the herein described co-expression of inhibitory and stimulatory receptors, emphasizes the dual role of CD8+ T cells in both tolerance and immunity. Co-expression of CD45RO/RA in several clusters hints at local proliferative potential, and interactions with APC and Treg may be essential to control CD8+ T cells at the maternal-fetal interface. Furthermore, recently addressed contributions of TCR $\gamma\delta$  T cells to transplantation outcomes and their role in HIV controllers (51, 52) advocates for an unexplored role of diverse subsets of TCR $\gamma\delta$  T cells in early and term pregnancy that requires further functional exploration. B cell clusters expressing CD39, a marker involved in the activation of B cells to suppress T cells (53), might resemble regulatory B cells. Alterations in B cell function in early pregnancy has been suggested to play a role in recurrent miscarriages, where a higher incidence of anti-HLA-C antibodies was observed in women with recurrent miscarriage (54).

Diffusion mapping revealed putative differentiation trajectories of effector, memory, and regulatory T cells throughout gestation, emphasizing the dynamic state and conceivable plasticity of decidua T cells in response to environmental cues. In both the CD4+ and CD8+ compartment an increase in activated effector T cell phenotypes towards the end of pregnancy suggests an inflammatory state required for parturition. Subsequently, combining all identified immune cell clusters in a correlation network analysis demonstrated that the local immune landscape as a whole, and not isolated cell subsets, develops into an integrated system throughout gestation. Co-expression of inhibitory and stimulatory receptors in this system is prominent and needs to be finely balanced to ensure a successful pregnancy. Differences in immune cell networks and their prospective functions observed between term basalis and decidua indicates possible distinct antigen availability and presentation at these two placental locations. More regulatory phenotypes were observed in the decidua with increased percentages of Treg, M2 M $\phi$ , and TRM CD8+ T cells. The abundant density of lymphatic vessels in the region adjacent to the chorionic membrane, which is attached to the decidua, suggests that antigen presentation and activation need to be carefully controlled at this site (55). Term basalis consistently showed cell clusters with higher expression of CCR6, a receptor

involved in chemotaxis. The influx of immune cells might therefore be more common in term basaloid.

This study has its limitations. First, in human pregnancy studies the unavailability of uncomplicated decidual samples between 24-37 weeks of gestation is a limitation that results in a gap in our knowledge and understanding of the complete second trimester. Second, mass cytometry identifies phenotypic diversity based on preselected markers and provides little insight into the functionality of identified cell clusters. Here, we investigated the T cells in depth, but additional myeloid and B cell-specific markers are necessary to explore the complexity within these lineages. Lastly, for future studies a validation cohort with additional healthy decidual samples and the inclusion of samples from complicated pregnancies will provide comprehensive insight into generalizable differences between healthy and pregnancy failure. Although, decidual and peripheral blood immune cells clustered completely separate in t-SNE analyses, trafficking of cells between these two entities almost certainly occurs (56, 57). In pregnancy complications both systems should be studied in parallel as the occurrence of certain cell subsets in the blood, possibly precursors, may predict what takes place locally in the decidua and thereby serve as biomarkers to predict complications.

In the field of reproductive immunology, a shift towards systems biology with a focus on interactions between cell types and away from studying isolated cell populations is required. This ecosystem where not only maternal immune cells but also EVT, decidual stromal cells, endothelial cells, and micro-organisms are coordinated with each other needs to be explored in more depth (27), and in relation to pregnancy complications that may present a more heterogeneous microenvironment than expected. Future studies will benefit from combining mass cytometry with single-cell RNA sequencing and imaging CyTOF to define the cellular anatomical locations. Furthermore, the generation of trophoblast organoids as a model for maternal-fetal interactions (58), development of a placenta-on-a-chip (59) and interconnectivity analysis of multiple biological systems such as metabolomics and transcriptomics (60, 27) will further enhance our understanding of the placenta and the cellular interactions within this ecosystem.

Taken together, mass cytometry enabled us to visualize the complex and dynamic network of immune cell populations at the maternal-fetal interface, where during uncomplicated pregnancy coordinated interaction between decidual cell types is vital for a successful outcome. The immune atlas as presented here may serve as a foundation for further identification and functional analyses of immune subsets in healthy versus complicated pregnancies.

## Materials and Methods

### Human decidual and blood samples

De-identified 1st and 2nd trimester human decidual material (gestational age 1st trimester, 6-13 weeks; 2nd trimester, 14-18 weeks) was obtained from women undergoing elective pregnancy termination. The gestational age was determined by ultrasonography and the tissue obtained by vacuum aspiration. Paired 3rd trimester (term) decidua basalis, decidua parietalis, and heparinized mPBMC were obtained from healthy women after uncomplicated pregnancy (gestational age >38 weeks) delivered by elective caesarean section or uncomplicated spontaneous vaginal delivery at Leiden University Medical Center (LUMC). Non-pregnant PBMC control samples were obtained from healthy females. The clinical characteristics of the subjects are shown in Table 1. All samples were obtained after informed consent and the study was carried out in accordance with the guidelines issued by the Medical Ethics Committee of the LUMC (protocols P08.087 and P11.196), and in accordance with the Declaration of Helsinki.

### Isolation of lymphocytes from decidual and PBMC samples

Decidual leukocytes were isolated as previously described, with some adjustments (61). For isolation of 1st and 2nd trimester decidual leukocytes, villous and decidual tissues from elective pregnancy terminations were macroscopically identified and separated. Decidua basalis and parietalis from term pregnancy were macroscopically dissected by scraping the basalis membrane from the placenta and by removing the amnion and delicately scraping the decidua parietalis from the chorion. Decidual tissues were washed with PBS, minced, and resuspended in Accutase cell detachment solution (prewarmed to 37°C; Gibco Life technologies). Subsequently, tissues were transferred to a C tube, homogenized on a gentle MACS dissociator (Miltenyi Biotec Ltd.) and incubated for 60 min in a water bath (37°C, gently shaking), at 30 min spinning the C tubes once more. After digestion, released cell suspensions were filtered through 250 µm and 70 µm sieves (Sigma-Aldrich; Miltenyi Biotec Ltd.) and washed with RPMI 1640 (Life technologies). Next, the cell suspensions were dissolved in 20 ml of 1.023 g/ml Percoll (GE Healthcare) and layered on a Percoll gradient (10ml 1.080g/ml; 15ml 1.053g/ml) for density gradient centrifugation (25min, 2000rpm). Leukocytes were isolated from the 1.080 - 1.053g/ml and the 1.053g/ml – 1.023g/ml interface, washed twice with RPMI, and left overnight at 4°C. Peripheral blood leukocytes were isolated from freshly drawn heparin anti-coagulated blood using Ficoll (GE Healthcare) density gradient centrifugation (20 min, 2000 rpm) and left overnight at 4°C. The next day, cell suspensions were incubated with Benzonase Nuclease (Sigma-Aldrich; 20U/mL) for 5 min, washed, counted and stained with antibodies for either mass cytometry or flow cytometry.

To account for cell processing variation, the effects of enzymatic digestion and gentleMACS dissociation on cell surface protein markers in peripheral blood and decidual cell suspensions has extensively been validated in our laboratory and by others (62).

### **Mass cytometry antibody staining and data acquisition**

Antibodies used for mass cytometry are listed in Table 2 and Table 3. Primary metal-conjugated antibodies were purchased from Fluidigm or purified antibodies were conjugated with metal reporters by using a MaxPar X8 Antibody Labeling kit (Fluidigm) according to manufacturer's instructions. After conjugation, antibodies were diluted to 200  $\mu$ l in antibody stabilization buffer (Candor Biosciences), supplemented with 0.05% sodium azide. Both antibody panels have previously been validated (63, 28), and in this study tested on both peripheral blood and decidual samples. Antibody staining and data acquisition were carried out as previously described (64, 22). In short, cells from decidual and peripheral blood samples were incubated with 1mL of 1:500 diluted 500uM Cell-ID Intercalator-103Rh (Fluidigm) for 15 min at room temperature (RT), washed and incubated with human Fc blocking antibody (Biolegend) for 10 min at RT. Cell suspensions were thereafter stained with a mix of metal-conjugated antibodies for 45 min at RT. After washing, cells were incubated with 125 nM Cell-ID Intercalator-Ir (Fluidigm) in MaxPar Fix and Perm buffer (Fluidigm) and left overnight at 4°C. Prior to data acquisition, cell pellets were diluted in distilled water containing 1:10 diluted EQ Four Element Calibration Beads (Fluidigm), and cells were acquired by a Helios mass cytometer (Fluidigm). After acquisition, data was normalized using the EQ beads with passport P13H2302 reference. To account for technical variation, a PBMC reference sample from a healthy donor was included for both the general and the T cell panel at ten intervals during 18 CyTOF acquisition runs over a time period of seven months (Fig. S2A, B).

### **Mass cytometry data analysis**

For each data file, live single CD45+ immune cells were selected by gating in Cytobank (Fig. S1A). The gating strategy utilized the parameters residual, event length, width and center to gate out debris and doublets. In addition, dead cells and normalization beads were excluded. Next, the files were subjected to sample-tagging, hyperbolic-arcsinh-transformation with cofactor 5 and dimensionality reduction in Cytosplore (24). Pair-wise Jensen-Shannon (JS) divergences were calculated for the individual samples within each tissue group, analyzed in a collective t-SNE, where low JS distances were indicative of high similarities between the samples within a group.

All data were pooled per panel and a five-level HSNE analysis was performed with default parameters (perplexity 30; iterations 1,000), where the major immune cell lineages were identified by automatic clustering (Fig. 1B, Fig. S1D, Fig. S2C). No influence of the mode of delivery on clustering of term decidual samples was observed in our analyses and a previous report by Tilburgs et al. (45) similarly confirmed no influence of mode of delivery

and other clinical variables on decidual cell types in term pregnancy. All HSNE, t-SNE, and Gaussian mean-shift clustering-derived cell clusters were generated in Cytosplore. Exported FCS files for all identified individual clusters were subjected to the CytoFast workflow in R (25). Hierarchical clustering of the heatmaps was created with Euclidean correction and average linkage and the median intensity values of markers were visualized. The number of cells in each immune cluster were determined for each sample and cluster frequencies and sample frequencies were calculated. Sample frequencies were visualized in boxplots and sample t-SNE plots. Violin plots, PCA plots and correlation network analysis were generated in R. Diffusion maps were generated in R using the 'destiny' package (33). Within the CD4+ T cell compartment, CD4+ TN cells together with the CD4+ TRORA cluster and Treg-like T cell clusters branched off completely and were omitted from the final CD4+ T cell diffusion map. Within the CD8+ T cell compartment, CD27-CD69-, CD27+CD69- TN and CD27<sup>INT</sup>CD69<sup>INT</sup>CD127+CCR6+ clusters branched off completely and were omitted from the final diffusion map. For the global test, incorporated within the Cytofast workflow, the absolute correlation distance with average linkage for hierarchical clustering was used. The branches colored in black show the significant multiplicity-corrected p-values.

### Flow Cytometry

Antibodies for flow cytometric analysis are listed in Table 5. For surface staining, cells were stained for 30 min at 4°C in PBS 1% FCS. For intracellular staining, cells were fixed and permeabilized using the FOXP3 staining buffer kit (eBioscience). Acquisition and analysis were performed on an LSR-II (BD Biosciences) using FACS Diva software. In addition, HSNE and t-SNE analysis of flow cytometric data was performed using Cytosplore. Co-expression of FOXP3, HELIOS, CTLA-4, CD39, ICOS, and TIGIT was confirmed by manual gating and HSNE analysis.

### Statistical analysis

Results are shown as median with interquartile range and the boxplots depict the 10-90 percentile. To determine differences among more than two unpaired groups, a non-parametric Kruskal-Wallis test with Dunn's multiple comparison post-test was applied where significance was assessed by controlling for false discovery at 5% (FDR). P-values < 0.05 were considered to denote statistically significant differences. Statistical analyses were performed in GraphPad Prism version 8.0 and R version 3.5.1.

### Data and materials availability

The mass cytometry datasets will be available via Flow Repository.

## **Acknowledgements**

We are thankful to the Center for Contraception, Abortion and Sexuality (CASA) in Leiden and The Hague, and Gynaikon in Rotterdam for their efforts in collecting and providing the decidual material. We thank all participating women; M. Nieveen, M. Bialecka, K. Lodder and T. van Herwaarden for dissection of decidual tissues; B. van der Goes and M. Tendeloo-Klarenbeek for collection of term placentas; J. Suwandi for assisting in setting up the T cell panel; T. Abdelaal, L. Na and J. Melsen for assisting with data analysis; G. Haasnoot for help with statistics.

## References

1. P. Velicky, M. Knöfler and J. Pollheimer. Function and control of human invasive trophoblast subtypes: Intrinsic vs. maternal control. *Cell Adhesion and Migration* 10:154-162, 2016.
2. S. Kovats, E. Main, C. Librach, M. Stubblebine, S. Fisher and DeMars R. A class I antigen, HLA-G, expressed in human trophoblasts. *Science* 248:220-223, 1990
3. A. King, D. S. Allan, M. Bowen, S. J. Powis, S. Joseph, S. Verma, S. E. Hiby, A. J. McMichael, Y. W. Loke and V. M. Braud. HLA-E is expressed on trophoblast and interacts with CD94/NKG2 receptors on decidual NK cells. *European Journal of Immunology* 30:1623-1631, 2000.
4. A. King, T. D. Burrows, S. E. Hiby, J. M. Bowen, S. Joseph, S. Verma, P. B. Lim, L. Gardner, P. Le Bouteiller, A. Ziegler, B. Uchanska-Ziegler and Y. W. Loke. Surface expression of HLA-C antigen by human extravillous trophoblast. *Placenta*. 21:376-387, 2000.
5. N. Gomez-Lopez, L. J. Guilbert and D. M. Olson. Invasion of the leukocytes into the fetal-maternal interface during pregnancy. *Journal of Leukocyte Biology* 88:625-633, 2010.
6. C. Bartmann, S. E. Segerer, L. Rieger, M. Kapp, M. Sütterlin and U. Kämmerer. Quantification of the Predominant Immune Cell Populations in Decidua Throughout Human Pregnancy. *American Journal of Reproductive Immunology* 71:109-119, 2014.
7. S. Liu, L. Diao, C. Huang, Y. Li, Y. Zeng and J. Y. Kwak-Kim. The role of decidual immune cells on human pregnancy. *Journal of Reproductive Immunology* 124:44-53, 2017.
8. J. Svensson-Arvelund and J. Ernerudh. The role of macrophages in promoting and maintaining homeostasis at the fetal-maternal interface. *American Journal of Reproductive Immunology* 74:100-109, 2015.
9. A. M. Sharkey, L. Gardner, S. Hiby, L. Farrell, R. Apps, L. Masters, J. Goodridge, L. Lathbury, C. A. Stewart, S. Verma and A. Moffett. Killer Ig-Like Receptor expression in uterine NK cells is biased toward recognition of HLA-C and alters with gestational age. *The Journal of Immunology* 181:39-46, 2008.
10. D. Lissauer, K. Piper, O. Goodyear, M. D. Kilby and P. A. H. Moss. Fetal-specific CD8+ cytotoxic T cell responses develop during normal human pregnancy and exhibit broad functional capacity. *The Journal of Immunology* 189:1072-1080, 2012.
11. T. Tilburgs and J. L. Strominger. CD8+ effector T cells at the fetal-maternal interface, balancing fetal tolerance and antiviral immunity. *American Journal of Reproductive Immunology* 69:395-407, 2013
12. R. M. Powell, D. Lissauer, J. Tamblyn, A. Beggs, P. Cox, P. Moss and M. D. Kilby. Decidual T cells exhibit a highly differentiated phenotype and demonstrate potential fetal specificity and a strong transcriptional response to IFN. *The Journal of Immunology* 199:3406-3417, 2017.
13. A. Steinborn, G. M. Haensch, K. Mahnke, E. Schmitt, A. Toerner, S. Meuer and C. Sohn. Distinct subsets of regulatory T cells during pregnancy: Is the imbalance of these subsets involved in the pathogenesis of preeclampsia? *Clinical Immunology* 129:401-412, 2008.
14. L. Rieger, S. Segerer, T. Bernar, M. Kapp, M. Majic, A. K. Morr, J. Dieltl and U. Kämmerer. Specific subsets of immune cells in human decidua differ between normal pregnancy and preeclampsia - a prospective observational study. *Reproductive Biology and Endocrinology* 7:132, 2009.
15. A. S. Bansal. Joining the immunological dots in recurrent miscarriage. *American Journal of Reproductive Immunology* 64:307-315, 2010.
16. K. Inada, T. Shima, A. Nakashima, K. Aoki, M. Ito and S. Saito. Characterization of regulatory T cells in decidua of miscarriage cases with abnormal or normal fetal chromosomal content. *Journal of Reproductive Immunology* 97:104-111, 2013.
17. N. Gomez-Lopez, D. StLouis, M. A. Lehr, E. N. Sanchez-Rodriguez and M. Arenas-Hernandez. Immune cells in term and preterm labor. *Cellular and Molecular Immunology* 11:571-581, 2014.
18. B. Gaudillière, E. A. Ganio, M. Tingle, H. L. Lancero, G. K. Fragiadakis, Q. J. Baca, N. Aghaepour, R. J. Wong, C. Quaintance, Y. Y. El-Sayed, G. M. Shaw, D. B. Lewis, D. K. Stevenson, G. P. Nolan and M. S. Angst. Implementing mass cytometry at the bedside to study the immunological basis of human diseases: Distinctive immune features in patients with a history of term or preterm birth. *Cytometry Part A* 87:817-829, 2015.

19. M. Arenas-Hernandez, R. Romero, Y. Xu, B. Panaitescu, V. Garcia-Flores, D. Miller, H. Ahn, B. Done, S. S. Hassan, C.-D. Hsu, A. L. Tarca, C. Sanchez-Torres and N. Gomez-Lopez. Effector and activated T cells induce preterm labor and birth that is prevented by treatment with progesterone. *The Journal of Immunology* 202:2585-2608, 2019.
20. T. Nagashima, Q. Li, C. Clementi, J. P. Lydon, F. J. DeMayo and M. M. Matzuk. BMP2 is required for post-implantation uterine function and pregnancy maintenance. *Journal of Clinical Investigation* 123:2539-2550, 2013.
21. D. R. Bandura, V. I. Baranov, O. I. Ornatsky, A. Antonov, R. Kinach, X. Lou, S. Pavlov, S. Vorobiev, J. E. Dick and S. D. Tanner. Mass cytometry: Technique for real time single cell multitarget immunoassay based on inductively coupled plasma time-of-flight mass spectrometry. *Analytical Chemistry* 81:6813-6822, 2009.
22. V. van Unen, N. Li, I. Molendijk, M. Temurhan, T. Höllt, A. E. van der Meulen-de Jong, H. W. Verspaget, M. L. Mearin, C. J. Mulder, J. van Bergen, B. P. Lelieveldt and F. Koning. Mass cytometry of the human mucosal immune system identifies tissue- and disease-associated immune subsets. *Immunity* 44:1227-1239, 2016.
23. V. Van Unen, T. Höllt, N. Pezzotti, N. Li, M. J. Reinders, E. Eisemann, F. Koning, A. Vilanova and B. P. Lelieveldt. Visual analysis of mass cytometry data by hierarchical stochastic neighbour embedding reveals rare cell types. *Nature Communications* 8:1740, 2017.
24. T. Höllt, N. Pezzotti, V. van Unen, F. Koning, E. Eisemann, B. Lelieveldt and A. Vilanova. Cytosplore: Interactive immune cell phenotyping for large single-cell datasets. *Computer Graphics Forum* 35:171-180, 2016.
25. G. Beyrend, K. Stam, T. Höllt, F. Ossendorp and R. Arens. Cytofast: A workflow for visual and quantitative analysis of flow and mass cytometry data to discover immune signatures and correlations. *Computational and Structural Biotechnology Journal* 16:435-442, 2018.
26. P. Vacca, L. Chiossone, M. C. Mingari and L. Moretta. Heterogeneity of NK cells and other innate lymphoid cells in human and murine decidua. *Frontiers in immunology* 10:170, 2019.
27. R. Vento-Tormo, M. Efremova, R. A. Botting, M. Y. Turco, M. Vento-Tormo, K. B. Meyer, J. E. Park, E. Stephenson, K. Polanski, A. Goncalves, L. Gardner, S. Holmqvist, J. Henriksson, A. Zou, A. M. Sharkey, B. Millar, B. Innes, L. Wood, A. Wilbrey-Clark, R. P. Payne, M. A. Ivarsson, S. Lisgo, A. Filby, D. H. Rowitch, J. N. Bulmer, G. J. Wright, M. J. Stubbington, M. Haniffa, A. Moffett and S. A. Teichmann. Single-cell reconstruction of the early maternal-fetal interface in humans. *Nature* 563:347-353, 2018.
28. N. Li, V. van Unen, T. Höllt, A. Thompson, J. van Bergen, N. Pezzotti, E. Eisemann, A. Vilanova, S. M. Chuva de Sousa Lopes, B. P. Lelieveldt and F. Koning. Mass cytometry reveals innate lymphoid cell differentiation pathways in the human fetal intestine. *The Journal of Experimental Medicine* 215:1383-1396, 2018.
29. J. P. Moorman, J. M. Wang, Y. Zhang, X. J. Ji, C. J. Ma, X. Y. Wu, Z. S. Jia, K. S. Wang and Z. Q. Yao. Tim-3 pathway controls regulatory and effector T cell balance during Hepatitis C Virus infection. *The Journal of Immunology* 189:755-766, 2012.
30. Y. Barsheshet, G. Wildbaum, E. Levy, A. Vitenshtein, C. Akinseye, J. Griggs, S. A. Lira and N. Karin. CCR8+ FOXP3+ Treg cells as master drivers of immune regulation. *Proceedings of the National Academy of Sciences* 114:6086-6091, 2017.
31. M. Gobert, I. Treilleux, N. Bendriss-Vermare, T. Bachelot, S. Goddard-Leon, V. Arfl, C. Biota, A. C. Doffin, I. Durand, D. Olive, S. Perez, N. Pasqual, C. Faure, I. Ray-Coquard, A. Puisieux, C. Caux, J. Y. Blay and C. Ménétrier-Caux. Regulatory T cells recruited through CCL22/CCR4 are selectively activated in lymphoid infiltrates surrounding primary breast tumors and lead to an adverse clinical outcome. *Cancer Research* 69:2000-2009, 2009.
32. N. Gagliani, C. F. Magnani, S. Huber, M. E. Gianolini, M. Pala, P. Licona-Limon, B. Guo, D. R. Herbert, A. Bulfone, F. Trentini, C. Di Serio, R. Bacchetta, M. Andreani, L. Brockmann, S. Gregori, R. A. Flavell and M. G. Roncarolo. Coexpression of CD49b and LAG-3 identifies human and mouse T regulatory type 1 cells. *Nature Medicine* 19:739-746, 2013.
33. L. Haghverdi, F. Buettner and F. J. Theis. Diffusion maps for high-dimensional single-cell analysis of differentiation data. *Bioinformatics* 31:2989-2998, 2015.
34. J. A. Saunders, K. A. Estes, L. M. Kosloski, H. E. Allen, K. M. Dempsey, D. R. Torres-Russotto, J. L. Meza, P. M. Santamaria, J. M. Bertoni, D. L. Murman, H. H. Ali, D. G. Standaert, R. L. Mosley and H. E. Gendelman. CD4+ regulatory and effector/memory T cell subsets profile motor dysfunction in Parkinson's disease. *Journal of Neuroimmune Pharmacology* 7:927-938, 2012.
35. A. van der Zwan, K. Bi, E. R. Norwitz, Á. C. Crespo, F. H. J. Claas, J. L. Strominger and T. Tilburgs. Mixed signature of activation and dysfunction allows human decidual CD8 + T cells to provide both tolerance and immunity. *Proceedings of the National Academy of Sciences* 115:385-390, 2018.

36. N. Chaturvedi, R. X. de Menezes and J. J. Goeman. A global  $\times$  global test for testing associations between two large sets of variables. *Biometrical Journal* 59:145-158, 2017.
37. J. Vazquez, M. Chavarria, Y. Li, G. E. Lopez and A. K. Stanic. Computational flow cytometry analysis reveals a unique immune signature of the human maternal-fetal interface. *American Journal of Reproductive Immunology* 79:e12774, 2018.
38. R. Slutsky, R. Romero, Y. Xu, J. Galaz, D. Miller, B. Done, A. L. Tarca, S. Gregor, S. S. Hassan, Y. Leng and N. Gomez-Lopez. Exhausted and senescent T cells at the maternal-fetal interface in preterm and term labor. *Journal of Immunology Research*, 2019: 3128010.
39. P. Vacca, L. Chiossone, M. C. Mingari and L. Moretta. Heterogeneity of NK cells and other innate lymphoid cells in human and murine decidua. *Frontiers in immunology* 10:170, 2019.
40. N. Aghaepour, E. A. Ganio, D. McIlwain, A. S. Tsai, M. Tingle, S. V. Gassen, D. K. Gaudilliere, Q. Baca, L. Mcneil, R. Okada, M. S. Ghaemi, D. Furman, R. J. Wong, V. D. Winn, M. L. Druzyn, Y. Y. El-Sayed, C. Quaintance, R. Gibbs, G. L. Darmstadt, G. M. Shaw, D. K. Stevenson, R. Tibshirani, G. P. Nolan, D. B. Lewis, M. S. Angst and B. Gaudilliere. An immune clock of human pregnancy. *Science Immunology* 2:2946, 2017.
41. J. Mjösberg, G. Berg, M. C. Jenmalm and J. Ernerudh. FOXP3+ regulatory T cells and T helper 1, T helper 2, and T helper 17 cells in human early pregnancy decidua. *Biology of reproduction* 82:698-705, 2010.
42. A. Kisielewicz, M. Schaier, E. Schmitt, F. Hug, G. M. Haensch, S. Meuer, M. Zeier, C. Sohn and A. Steinborn. A distinct subset of HLA-DR+ regulatory T cells is involved in the induction of preterm labor during pregnancy and in the induction of organ rejection after transplantation. *Clinical immunology* 137:209-220, 2010.
43. M. Salvany-Celades, A. van der Zwan, M. Benner, V. Setrajic-Dragos, H. A. Bougleux Gomes, V. Iyer, E. R. Norwitz, J. L. Strominger and T. Tilburgs. Three types of functional regulatory T cells control T cell responses at the human maternal-fetal interface. *Cell Reports* 27:2537-2547, 2019.
44. W. Zeng, Z. Liu, X. Liu, S. Zhang, A. Khanniche, Y. Zheng, X. Ma, T. Yu, F. Tian, X. R. Liu, J. Fan and Y. Lin. Distinct transcriptional and alternative splicing signatures of decidual CD4+ T cells in early human pregnancy. *Frontiers in Immunology* 8:682, 2017.
45. T. Tilburgs, S. A. Scherjon, B. J. van der Mast, G. W. Haasnoot, M. Versteeg-v.d.Voort-Maarschalk, D. L. Roelen, J. J. van Rood and F. H. Claas. Fetal-maternal HLA-C mismatch is associated with decidual T cell activation and induction of functional T regulatory cells. *Journal of Reproductive Immunology* 82:148-157, 2009.
46. S. Tsuda, X. Zhang, H. Hamana, T. Shima, A. Ushijima, K. Tsuda, A. Muraguchi, H. Kishi and S. Saito. Clonally expanded decidual effector regulatory T cells increase in late gestation of normal pregnancy, but not in preeclampsia, in humans. *Frontiers in Immunology* 9:1934, 2018.
47. S. Tsuda, A. Nakashima, T. Shima and S. Saito. New paradigm in the role of regulatory T cells during pregnancy. *Frontiers in Immunology* 10:573, 2019.
48. J. Yuan, J. Li, S. Y. Huang and X. Sun. Characterization of the subsets of human NKT-like cells and the expression of Th1/Th2 cytokines in patients with unexplained recurrent spontaneous abortion. *Journal of Reproductive Immunology* 110:81-88, 2015.
49. A. van Egmond, C. van der Keur, G. M. J. S. Swings, S. A. Scherjon and F. H. J. Claas. The possible role of virus-specific CD8+ memory T cells in decidual tissue. *Journal of Reproductive Immunology* 113:1-8, 2016.
50. A. van der Zwan, E. M. van der Meer-Prins, P. P. van Miert, H. van den Heuvel, J. D. Anholts, D. L. Roelen, F. H. Claas and S. Heidt. Cross-reactivity of virus-specific CD8+ T cells against allogeneic HLA-C: Possible implications for pregnancy outcome. *Frontiers in immunology* 9:2880, 2018.
51. O. McCallion, J. Hester and F. Issa. Deciphering the contribution of  $\gamma\delta$  T cells to outcomes in transplantation. *Transplantation* 102:1983-1993, 2018.
52. M. F. Chevalier, N. Bhatnagar, C. Didier, M. Lopez-Gonzalez, J. Pavie, D. Bollens, C. Duvivier, L. Collias, C. Jung, D. Scott-Algara, P.-M. Girard and L. Weiss.  $\gamma\delta$  T cells subsets in HIV controllers: potential role of T $\gamma\delta$ 17 cells in the regulation of chronic immune activation. *AIDS* 33:1283-1292, 2019.
53. Z. Saze, P. J. Schuler, C. S. Hong, D. Cheng, E. K. Jackson and T. L. Whiteside. Adenosine production by human B cells and B cell-mediated suppression of activated T cells. *Blood* 122:9-18, 2013.
54. T. Meuleman, E. van Beelen, R. J. Kaaja, J. M. van Lith, F. H. Claas and K. W. Bloemenkamp. HLA-C antibodies in women with recurrent miscarriage suggests that antibody mediated rejection is one of the mechanisms leading to recurrent miscarriage. *Journal of Reproductive Immunology* 116:28-34, 2016.

55. O. Genbacev, L. Vicovac and N. Larocque. The role of chorionic cytotrophoblasts in the smooth chorion fusion with parietal decidua. *Placenta* 36:716-722, 2015.
56. C. Carlino, H. Stabile, S. Morrone, R. Bulla, A. Soriani, C. Agostinis, F. Bossi, C. Mocchi, F. Sarazani, F. Tedesco, A. Santoni and A. Gismondi. Recruitment of circulating NK cells through decidual tissues: a possible mechanism controlling NK cell accumulation in the uterus during early pregnancy. *Blood* 111:3108-3115, 2008.
57. M.R. Du, S.C. Wang and D.J. Li. The integrative roles of chemokines at the maternal-fetal interface in early pregnancy. *Cellular & molecular immunology* 11:438-448, 2014.
58. M. Y. Turco, L. Gardner, R. G. Kay, R. S. Hamilton, M. Prater, M. S. Hollinshead, A. McWhinnie, L. Esposito, R. Fernando, H. Skelton, F. Reimann, F. M. Gribble, A. Sharkey, S. G. Marsh, S. O'rahilly, M. Hemberger, G. J. Burton and A. Moffett. Trophoblast organoids as a model for maternal-fetal interactions during human placentation. *Nature* 564:263-281, 2018.
59. J. S. Lee, R. Romero, Y. M. Han, H. C. Kim, C. J. Kim, J. S. Hong and D. Huh. Placenta-on-A-chip: A novel platform to study the biology of the human placenta. *Journal of Maternal-Fetal and Neonatal Medicine* 29:1046-1054, 2016.
60. M. S. Ghaemi, D. B. DiGiulio, K. Contrepois, B. Callahan, T. T. Ngo, B. Lee-McMullen, B. Lehallier, A. Robaczewska, D. McIlwain, Y. Rosenberg-Hasson, R. J. Wong, C. Quaintance, A. Culos, N. Stanley, A. Tanada, A. Tsai, D. Gaudilliere, E. Ganio, X. Han, K. Ando, L. McNeil, M. Tingle, P. Wise, I. Maric, M. Sirota, T. Wyss-Coray, V. D. Winn, M. L. Druzin, R. Gibbs, G. L. Darmstadt, D. B. Lewis, V. Partovi Nia, B. Agard, R. Tibshirani, G. Nolan, M. P. Snyder, D. A. Relman, S. R. Quake, G. M. Shaw, D. K. Stevenson, M. S. Angst, B. Gaudilliere and N. Aghaepour. Multiomics modeling of the immunome, transcriptome, microbiome, proteome and metabolome adaptations during human pregnancy. *Bioinformatics* 35:95-103, 2019.
61. T. Tilburgs, Á. C. Crespo, A. van der Zwan, B. Rybalov, T. Raj, B. Stranger, L. Gardner, A. Moffett and J. L. Strominger. Human HLA-G+ extravillous trophoblasts: Immune-activating cells that interact with decidual leukocytes. *Proceedings of the National Academy of Sciences* 112:7219-7224, 2015.
62. Y. Xu, O. Plazyo, R. Romero, S. S. Hassan and N. Gomez-Lopez. Isolation of leukocytes from the human maternal-fetal interface. *Journal of Visualized Experiments* e52863, 2015.
63. S. Laban, J. S. Suwandi, V. Van Unen, J. Pool, J. Wesselius, T. Höllt, N. Pezzotti, A. Vilanova, B. P. Lelieveldt and B. O. Roep. Heterogeneity of circulating CD8 T-cells specific to islet, neo-antigen and virus in patients with type 1 diabetes mellitus. *PLoS ONE* 13:e0200818, 2018.
64. S. C. Bendall, E. F. Simonds, P. Qiu, E.-A. D. Amir, P. O. Krutzik, R. Finck, R. V. Bruggner, R. Melamed, A. Trejo, O. I. Ornatsky, R. S. Balderas, S. K. Plevritis, K. Sachs, D. Pe'er, S. D. Tanner and G. P. Nolan. Single-cell mass cytometry of differential immune and drug responses across a human hematopoietic continuum. *Science* 332:687-696, 2011.

## Supplemental Information

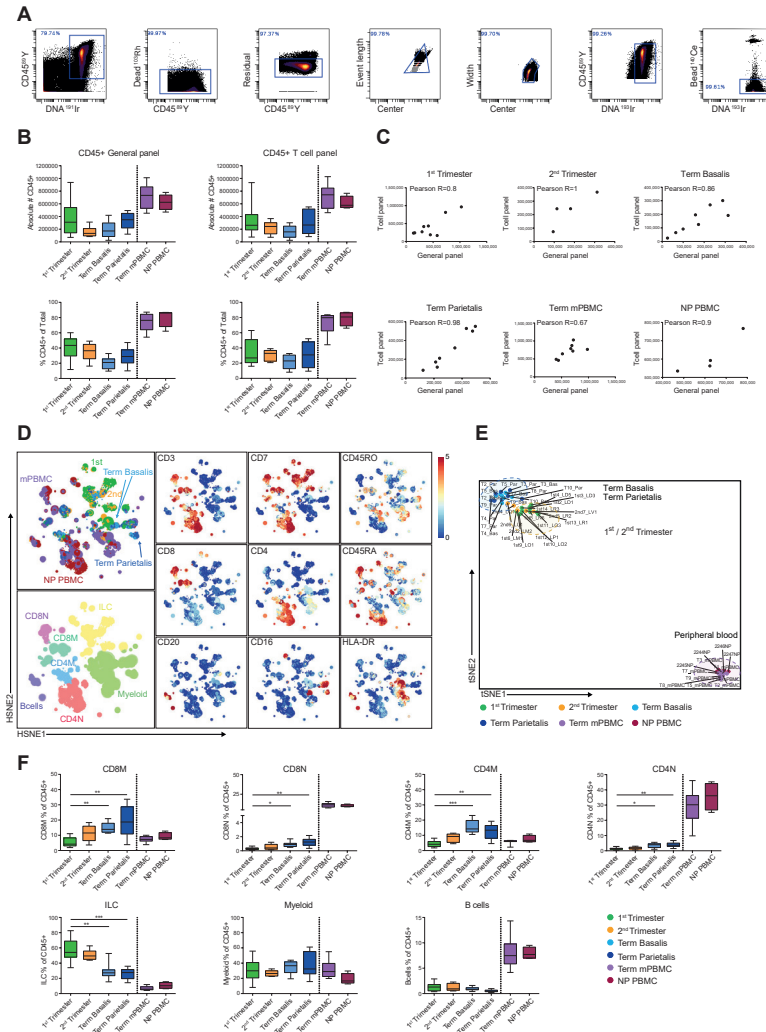


**Figure S1. Identification of major immune cell lineages at the maternal-fetal interface using the T cell panel.**

(A) Gating strategy to select single, live CD45<sup>+</sup> cells for downstream analysis. (B) Comparison of the absolute numbers and percentages of CD45<sup>+</sup> cells measured by the general and the T cell panel. (C) Correlation plots of CD45<sup>+</sup> cells measured by the general and T cell panel within the three trimesters, maternal peripheral blood mononuclear cells (mPBMC) and non-pregnant control samples (NP PBMC). (D) First-level HSNE visualization of the major immune cell lineages derived from decidua and peripheral blood. Colors top left indicate tissue type (1<sup>st</sup> trimester n = 11; 2<sup>nd</sup> trimester n = 5; term basalis and parietalis n = 8; mPBMC n = 8; NP PBMC n = 4); colors bottom left indicate major immune cell types (CD8M, CD8 memory T cells; CD8N, CD8 naive T cells; CD4M, CD4 memory T cells; CD4N, CD4 naive T cells); colors for plots on the right indicate the arcSinh5-transformed expression values of the specified markers where every dot represents a landmark. (E) t-SNE visualization of the separation between decidual and peripheral blood samples (as percentage of CD45<sup>+</sup> cells); every dot represents a single sample. (F) Major immune cell lineages (as percentage of CD45<sup>+</sup> cells) throughout gestation and within mPBMC and NP PBMC. Boxplots depict the 10-90 percentile and the Kruskal-Wallis with Dunn's test for multiple comparisons was applied. \*P < 0.05; \*\*P < 0.01; \*\*\*P < 0.001.

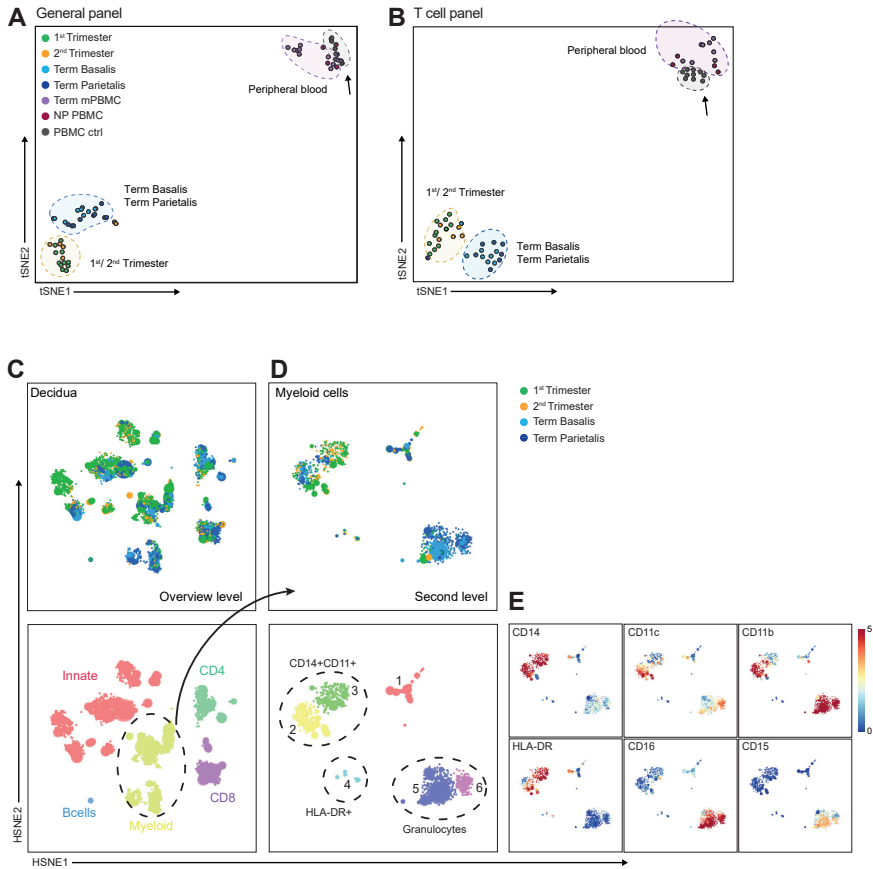


**Figure S2. t-SNE visualization of PBMC reference samples and partitioning of the myeloid cell compartment into subpopulations.**

Cell frequencies (as percentage of CD45+ cells) are plotted where every dot represents a single sample within the general panel (A) and within the T cell panel (B). The grey arrow indicates the PBMC reference control samples clustering together. (C) HSNE overview (first) level embedding of all decidua samples with identification of the major immune cell lineages based on lineage marker expression. (D) Second-level HSNE embedding of the myeloid cells subdivided into six major subpopulations. (E) Second-level HSNE arcSinh5-transformed expression values of the specified markers where every dot represents a landmark..

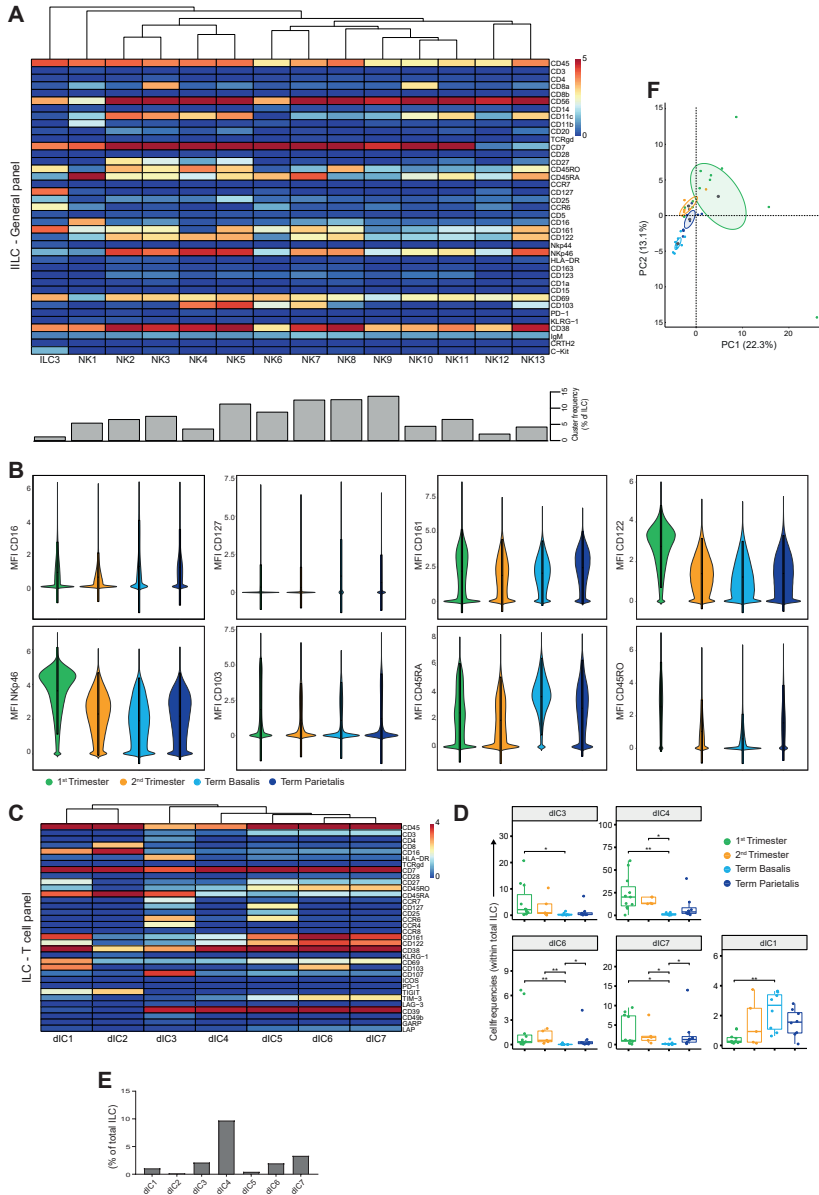


**Figure S3. Characterization of the innate lymphoid compartment.**

(A) Heatmap showing the marker expression values for the 14 identified NK and ILC clusters. Cluster IDs and cluster frequencies are displayed at the bottom of the heatmap. (B) Violin plots depicting expression values of indicated markers (arcSinh5-transformed) in the four tissue groups. (C) Heatmap showing the marker expression values for ILC clusters (CD3-CD7+) within the T cell panel. Only clusters expressing the co-inhibitory receptors CD39, TIM-3, TIGIT are depicted here. (D) Boxplots of sample frequencies, divided per trimester, of the clusters plotted as a fraction of total ILCs. The Kruskal-Wallis with Dunn's test for multiple comparisons was performed. (E) Cluster frequencies (as percentage of total ILC) of the depicted clusters. (F) PCA of the sample frequencies (as percentage of total ILCs) where the gestational age groups are depicted along the first two components. The centroid of each group is indicated in grey. \*  $P \leq 0.05$ ; \*\*  $P \leq 0.01$ ; \*\*\*  $P \leq 0.001$ .

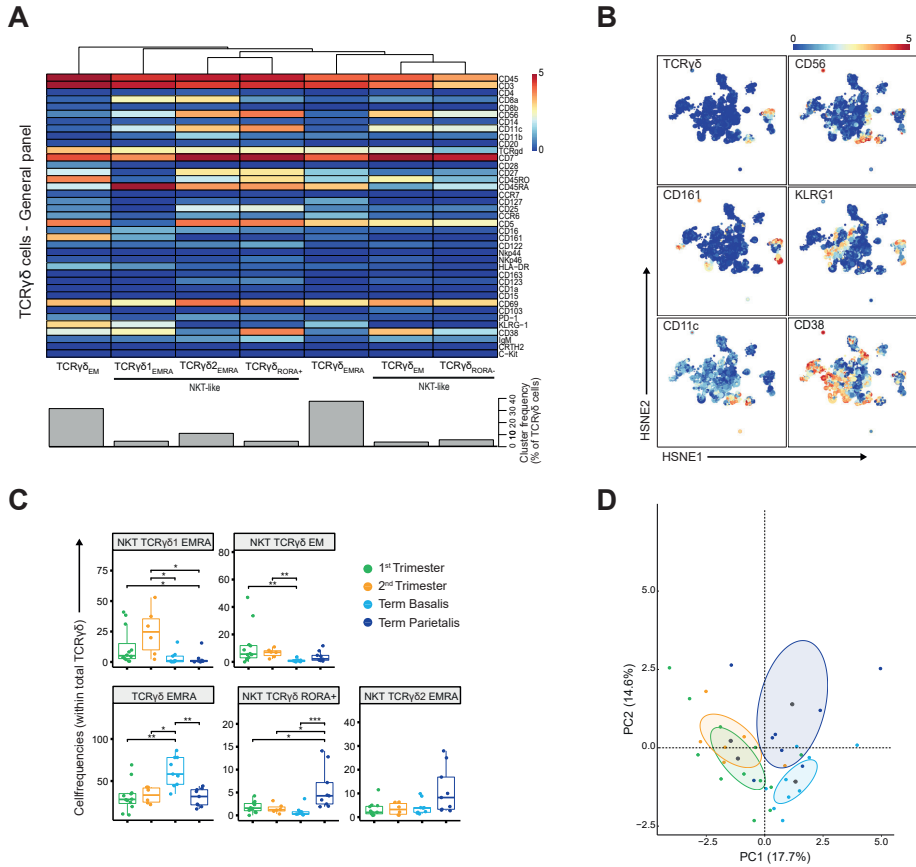
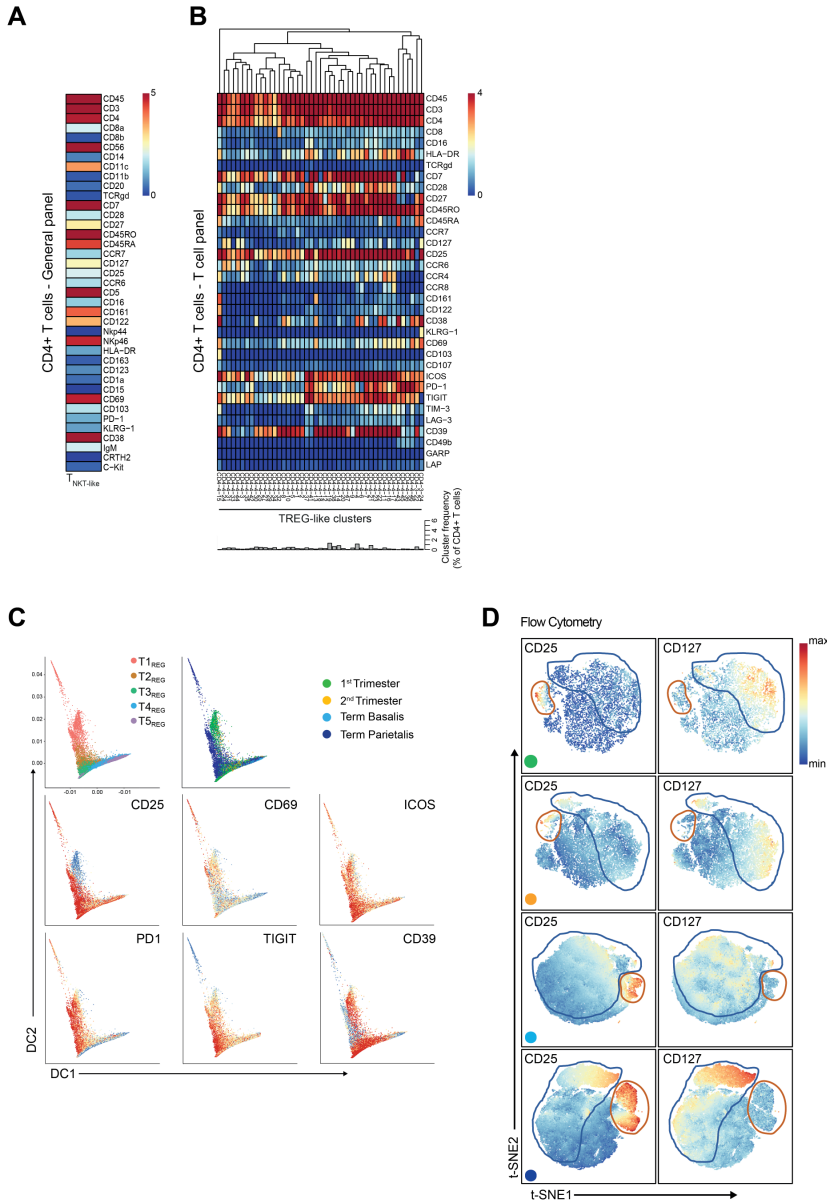


**Figure S4. Characterization of the TCR $\gamma\delta$  T cells.**

(A) Heatmap showing the marker expression values for the seven identified TCR $\gamma\delta$  cell clusters within the general panel (36 samples; 114,875 cells). Cluster IDs and cluster frequencies are displayed at the bottom of the heatmap. (B) First-level HSNE embedding of the expression values of the indicated markers. (C) Box-plots of sample frequencies, divided per trimester, of the clusters plotted as a fraction of total TCR $\gamma\delta$  cells. The Kruskal-Wallis with Dunn's test for multiple comparisons was performed. (D) PCA of the sample frequencies (as percentage of total TCR $\gamma\delta$  cells) where the gestational age groups are depicted along the first two components. The centroid of each group is indicated in grey. \*  $P \leq 0.05$ ; \*\*  $P \leq 0.01$ ; \*\*\*  $P \leq 0.001$ .



07

**Figure S5. In-depth characterization of the CD4+ Treg-like compartment where CD25+CD127- and CD25+CD127+ CD4+ T cells increase throughout gestation.**

(A) CD4+ NKT-like cell cluster identified within the general panel. (B) In-depth analysis of the regulatory-like CD4+ T cell (Treg-like) compartment, where the heatmap shows the marker expression values for the additional identified CD4+ Treg-like cell clusters within the T cell panel. Cluster IDs and cluster frequencies are displayed at the bottom of the heatmap. (C) Visualization of the five CD4+ Treg-like clusters, shown in Fig. 3A, in a diffusion map along two components. Each color in the left panel represents a cluster of cells. In the right top panel, cells within the 1st trimester, 2nd trimester, and term decidua basalis and parietalis are portrayed. The bottom panel shows expression values of the specified markers in the diffusion map. (D) t-SNE embedding of the arcSinh-transformed expression values of CD127 and CD25 as observed in the three trimesters, measured by flow cytometry and gated within CD3+CD4+ T cells.



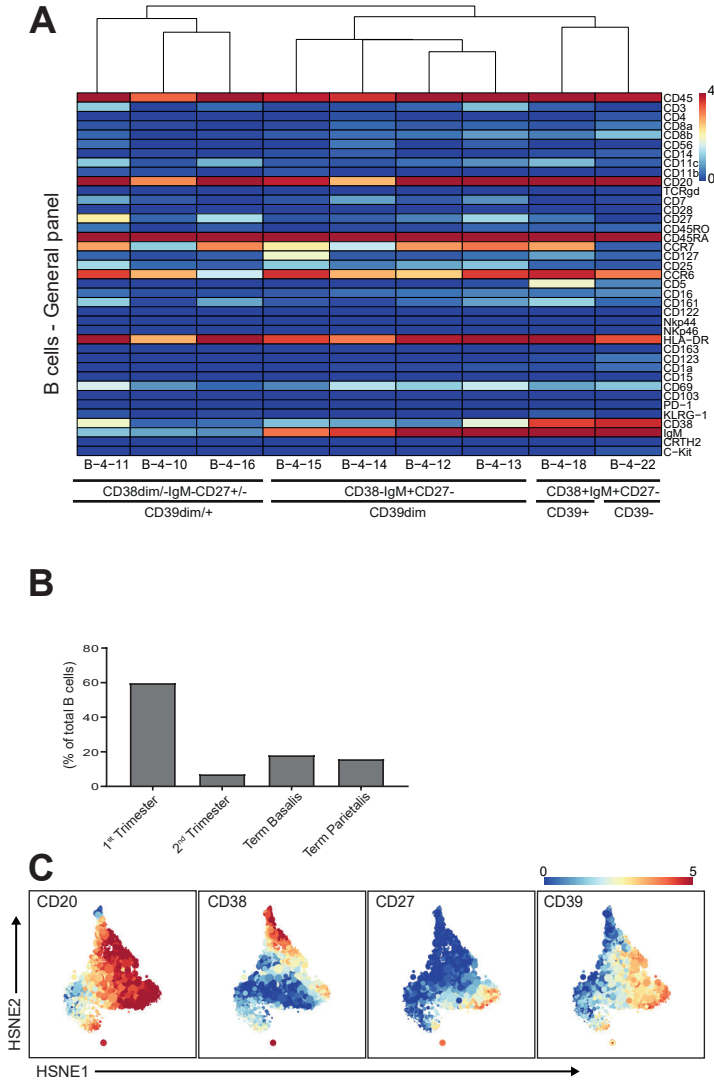


**Figure S7. Characterization of B cells.**

(A) Heatmap showing the marker expression values for the nine identified B cell clusters within the general panel (36 samples; 72,414 cells). (B) Percentage of CD20+ B cells in each trimester. (C) ArcSinh5-transformed expression values of the specified markers. \*  $P \leq 0.05$ ; \*\*  $P \leq 0.01$ ; \*\*\*  $P \leq 0.001$ .

	1st trimester	2nd trimester	3rd trimester	NP PBMC
<b>Demographics</b>				
Maternal age (years; mean $\pm$ SD)	Unknown	Unknown	32.8 $\pm$ 4.3	30.5 $\pm$ 3.1
Body mass index (BMI; mean $\pm$ SD)	Unknown	Unknown	25.4 $\pm$ 3.9	22.1 $\pm$ 0.4
Gravity (median, IQR)	Unknown	Unknown	2 (1, 2)	0
Parity (% nulliparous)	Unknown	Unknown	46	100
<b>Pregnancy parameters</b>				
Gestational age (weeks; mean $\pm$ SD)	9.2 $\pm$ 2.1	15.5 $\pm$ 1.2	39.1 $\pm$ 0.8	NA
Placenta weight (kg; mean $\pm$ SD)	NA	NA	564.5 $\pm$ 87.3	NA
Mode of delivery	Elective abortion	Elective abortion	Spontaneous + C-section	NA
Sex of child (%)	M 53.8%/ F 46.2%	M 9.1%/ F 90.9%	M 53.8%/ F 46.2%	NA
<b>Experiment inclusions</b>				
General CyTOF panel	n = 12	n = 6	n = 9	n = 4
T cell CyTOF panel	n = 11	n = 5	n = 8	n = 4
FACS panel	n = 3	n = 4	n = 4	NA

**Table 1. Patient characteristics.**

IQR, interquartile range

\*All pregnancies were considered healthy as determined by demographics, pregnancy parameters, attending gynaecologist-obstetrician and research nurses, and absence of membrane discoloration and infarctions.

\*For some elective termination samples, the sex could not be determined.

	Antigen	Tag	Clone	Company	Cat#
1	CD8a	<sup>146</sup> Nd	RPA-T8	Fluidigm	3146001B
2	CD11c	<sup>162</sup> Dy	Bu15	Fluidigm	3162005B
3	CD127	<sup>165</sup> Ho	AO19D5	Fluidigm	3165008B
4	CD38	<sup>172</sup> Yb	HIT2	Fluidigm	3172007B
5	CD69	<sup>144</sup> Nd	FN50	Fluidigm	3144018B
6	CD11b	<sup>209</sup> Bi	ICRF44	Fluidigm	3209003B
7	CD45	<sup>89</sup> Y	HI30	Fluidigm	3089003B
8	CCR6	<sup>141</sup> Pr	G034E3	Fluidigm	3141003A
9	C-Kit	<sup>143</sup> Nd	104D2	Fluidigm	3143001B
10	CD4	<sup>145</sup> Nd	RPA-T4	Fluidigm	3145001B
11	CD16	<sup>148</sup> Nd	3G8	Fluidigm	3148004B
12	CD25	<sup>149</sup> Sm	2A3	Fluidigm	3149010B
13	CD123	<sup>151</sup> Eu	6H6	Fluidigm	3151001B
14	CD7	<sup>153</sup> Eu	CD7-6B7	Fluidigm	3153014B
15	CD163	<sup>154</sup> Sm	GHI/61	Fluidigm	3154007B
16	CCR7	<sup>159</sup> Tb	G043H7	Fluidigm	3159003A
17	CD161	<sup>164</sup> Dy	HP-3G10	Fluidigm	3164009B
18	CD27	<sup>167</sup> Er	O323	Fluidigm	3167002B
19	CD45RA	<sup>169</sup> Tm	HI100	Fluidigm	3169008B
20	CD3	<sup>170</sup> Er	UCHT1	Fluidigm	3170001B
21	PD-1	<sup>175</sup> Lu	EH 12.2H7	Fluidigm	3175008B
22	CD56	<sup>176</sup> Yb	NCAM16.2	Fluidigm	3176008B
23	TCRgd	<sup>152</sup> Sm	11F2	Fluidigm	3152008B
24	CD15	<sup>115</sup> In	W6D3	Biolegend	323035
25	CD1a	<sup>142</sup> Nd	HI149	Sony	2100510
26	CD5	<sup>160</sup> Gd	UCHT2	Biolegend	300627
27	HLA-DR	<sup>168</sup> Er	L243	Biolegend	307651
28	IgM	<sup>150</sup> Nd	MHM88	Biolegend	314527
29	CD103	<sup>155</sup> Gd	Ber-ACT8	Biolegend	350202
30	CRTH2	<sup>156</sup> Gd	BM16	Biolegend	350102
31	CD20	<sup>163</sup> Dy	2H7	Biolegend	302343
32	CD28	<sup>171</sup> Yb	CD28.2	Biolegend	302937
33	CD45RO	<sup>173</sup> Yb	UCHL1	Biolegend	304239
34	CD122	<sup>158</sup> Gd	TU27	Biolegend	339015
35	KLRG-1	<sup>161</sup> Dy	REA261	MACS	120-014-229
36	CD8b	<sup>166</sup> Er	SID18BEE	Ebioscience	14-5273
37	NKp46	<sup>174</sup> Yb	9E 2	Biolegend	331902
38	Nkp44	<sup>147</sup> Sm	253415	R&D Systems	MAB22491
39	CD14	Qdot800	Tük4	ThermoFisher/Invitrogen	Q10064

Table 2. General CyTOF antibody panel.

\*36 antibodies published in 'Na Li et al. 2018' [28], with addition of CD69, CD5, CD15, and CD1a.

1	CD3	<sup>161</sup> Dy	UCHT1	Biologend	300443
2	CD4	<sup>145</sup> Nd	RPA-T4	Fluidigm	3145001B
3	CD7	<sup>166</sup> Er	M-T701	Fluidigm	3166027B
4	CD8a	<sup>146</sup> Nd	RPA-T8	Fluidigm	3146001B
5	CD16	<sup>148</sup> Nd	3G8	Fluidigm	3148004B
6	CD20	<sup>163</sup> Dy	2H7	Biologend	302343
7	CD25	<sup>149</sup> Sm	2A3	Fluidigm	3149010B
8	CD27	<sup>167</sup> Er	O323	Fluidigm	3167002B
9	CD28	<sup>171</sup> Yb	CD28.2	Biologend	302902
10	CD38	<sup>172</sup> Yb	HIT2	Fluidigm	3172007B
11	CD39	<sup>162</sup> Dy	A1	Biologend	328202
12	CD45	<sup>89</sup> Y	HI30	Fluidigm	3089003B
13	GARP	<sup>169</sup> Tm	7B11	Biologend	353502
14	CD45RO	<sup>173</sup> Yb	UCHL1	Biologend	304239
15	CD49b	<sup>176</sup> Yb	P1e6c5	Biologend	359301
16	CD69	<sup>144</sup> Nd	FN50	Fluidigm	3144018B
17	CD103	<sup>155</sup> Gd	Ber-ACT8	Biologend	350202
18	CD107	<sup>143</sup> Nd	H4A3	Biologend	14-1079
19	CD122	<sup>158</sup> Gd	TU27	Biologend	339002
20	CD127	<sup>165</sup> Ho	AO19D5	Fluidigm	3165008B
21	CTLA-4*	<sup>170</sup> Er	14D3	Fluidigm	3170005B
22	CD161	<sup>164</sup> Dy	HP-3G10	Fluidigm	3164009B
23	CCR4	<sup>156</sup> Gd	L291H4	Biologend	359402
24	CCR6	<sup>141</sup> Pr	G034E3	Fluidigm	3141003A
25	CCR7	<sup>142</sup> Nd	G043H7	Biologend	353237
26	PD-1	<sup>175</sup> Lu	EH 12.2H7	Fluidigm	3175008B
27	LAG3	<sup>150</sup> Nd	874501	Fluidigm	3150016B
28	ICOS	<sup>151</sup> Eu	C398.4A	Fluidigm	3151020B
29	CCR8	<sup>147</sup> Sm	L263G8	Biologend	360602
30	LAP	<sup>174</sup> Yb	TW4-2F8	Biologend	349602
31	GITR*	<sup>159</sup> Tb	621	Fluidigm	3159020B
32	TIM-3	<sup>154</sup> Sm	F38-2E2	Fluidigm	3154010B
33	TIGIT	<sup>153</sup> Eu	MBSA43	Fluidigm	3153019B
34	HLA-DR	<sup>168</sup> Er	L243	Biologend	307651
35	TCRgd	<sup>152</sup> Sm	11F2	Fluidigm	3152008B
36	KLRG1	<sup>160</sup> Gd	REA261	Miltenyi	120-014-229
37	CD45RA	Qdot655	MEM-56	ThermoFisher/Invitrogen	Q10069

**Table 3. T cell-specific CyTOF antibody panel.**

Part of mass cytometry panel published in 'Laban et al. 2018' (63).

\*GITR and CTLA-4 antibodies, although validated, did not show expression in decidual samples

	# of Decidual samples	CD4+ T cells	CD8+ T cells	B cells	Myeloid cells	ILC/NK cells	TCRγδ cells
General panel	36	1,136,799	1,082,234	72,414	2,390,451	3,841,125	114,875
T cell panel	32	818,800	707,147	73,579	2,087,932	3,556,369	96,640

Trimester	Total # of samples	General panel	T cell panel	% Overlap
1st Basalis	14	12	11	9; 64%
2nd Basalis	7	6	5	4; 57%
3rd Basalis	9	9	8	8; 89%
3rd Parietalis	9	9	8	8; 89%
mPBMC	9	9	8	8; 89%
NP PBMC	4	4	4	4; 100%

Table 4. Total number of cells and samples measured.

\*36 antibodies published in 'Na Li et al. 2018' (28), with addition of CD69, CD5, CD15, and CD1a.

	Antigen	Fluorochrome	Clone	Company	Cat#
<b>Extracellular</b>					
1	CD45	Krome Orange	J.33	Beckman Coulter	B36294
2	CD3	ECD	UCHT1	Beckman Coulter	A07748
3	CD3	PE	SK7	BD Biosciences	345765
4	CD4	A700	RPA-T4	BD Biosciences	557922
5	CD8	Pacific Blue	RPA-T8	BD Biosciences	558207
6	CD127	PerCP-Cy5.5	A019D5	Biolegend	351321
7	CD25	PE	2A3	BD Biosciences	341011
8	ICOS	APC-Cy7	C398.4A	Biolegend	313529
9	TIGIT	APC	MBSA43	Invitrogen	17-9500-41
10	CD39	BV510	A1	Biolegend	328219
11	PD-1	PE-Cy7	EH12.1	BD Biosciences	561272
12	CD69	PE	FN50	BD Biosciences	555531
13	CCR7	A488	G043H7	Biolegend	353206
14	CD45RA	PE-TexasRed	MEM-56	Life Technologies	MHCD45RA17
<b>Intracellular</b>					
15	FOXP3	FITC	PCH101	Invitrogen	11-4776-71
16	HELIOS	Pacific Blue	22F6	Biolegend	137220
17	CTLA-4	PE-Cy7	L3D10	Biolegend	349913

Table 5. Flow cytometry antibody panel.

\*Matched IgG controls were included

07

